UNIVERSIDAD DE CONCEPCIÓN

Centro de Investigación en Ingeniería Matemática (CI^{2}MA)

A hybrid stochastic Galerkin method for uncertainty quantification applied to a conservation law modelling a clarifier-thickener unit

Raimund Bürger, Ilja Kröker,
Christian Rohde

PREPRINT 2012-23

SERIE DE PRE-PUBLICACIONES

A hybrid stochastic Galerkin method for uncertainty quantification applied to a conservation law modelling a clarifier-thickener unit

Raimund Bürger[1], **Ilja Kröker**[2], **and Christian Rohde**[2]

[1] CI^{2}MA and Departamento de Ingeniería Matemática, Universidad de Concepción, Casilla 160-C, Concepcion, Chile, rburger@ing-mat.udec.cl

[2] IANS, Universität Stuttgart, Pfaffenwaldring 57, D-70569 Stuttgart, Germany, ikroeker|crohde@mathematik.uni-stuttgart.de

Received XXXX, revised XXXX, accepted XXXX
Published online XXXX

Key words clarifier-thickener model, polynomial chaos, uncertainty quantification, Galerkin projection, finite volume method

MSC (2000) 00-xx

The continuous sedimentation process in a clarifier-thickener can be described by a scalar nonlinear conservation law for the local solids volume fraction. The flux density function is discontinuous with respect to spatial position due to feed and discharge mechanisms. Typically, the feed flow cannot be given deterministically and efficient numerical simulation requires a concept for quantifying uncertainty.
In this paper uncertainty quantification is expressed by a new hybrid stochastic Galerkin (HSG) method that extends the classical polynomial chaos approximation by multiresolution discretization in the stochastic space. The new approach leads to a deterministic hyperbolic system for a finite number of stochastic moments which is however partially decoupled and thus allows efficient parallelisation. The complexity of the problem is further reduced by stochastic adaptivity.
For the approximate solution of the resulting high-dimensional system a finite volume scheme is introduced. Numerical experiments cover one- and two-dimensional situations.

1 Introduction

1.1 Scope

Modelling uncertainty is important in many technical applications in which one seeks to quantify the stochastic variability of the response of a nonlinear system, usually defined by the solution of a time-dependent partial differential equation (PDE), with respect to uncertainty in input data such as initial conditions, control parameters and PDE coefficient functions. Straightforward Monte-Carlo (MC) computations of sampling solutions produced under stochastic variation of the input data are easily implemented, but quantifying randomness via the MC approach is computationally very inefficient due to the slow convergence of stochastics. However we refer to the Multi-Level Monte-Carlo [30] and Quasi Monte-Carlo [24] for the variants of the improvement. The quantification of randomness by stochastic Galerkin or collocation methods leads to deterministic models for at least a finite number of stochastic moments (cf. [29] for an overview), and seems to be a more promising technique in the present situation. While this approach is supported by a meanwhile well-understood theory for models posed in terms of linear PDEs, for nonlinear problems first steps have been done just recently [1, 32, 36, 37]. One important subclass of nonlinear problems are hyperbolic conservation laws, on which the present work is focused.

As a prototype model in this field we consider a clarifier-thickener (CT) model for the continuous fluid-solid separation of suspensions under gravity. The CT model provides an idealized description of secondary settling tanks in wastewater treatment or of thickeners in mineral processing [7]. For so-called ideal suspensions of small solid, non-flocculent particles that do not exhibit the effect of sediment compressibility, the complete set of governing partial differential equations is given by a first-order scalar conservation law for the local solids concentration that involves as a coefficient the local volume-averaged flow velocity of the mixture (in short, bulk velocity); this velocity must satisfy a divergence-free condition plus possibly an additional equation of motion [12, 13]. It is frequently assumed, however, that all variables are horizontally constant such that a spatially one-dimensional description is sufficient. Then the governing equation is one single scalar conservation law with a flux density function that depends spatially on position, along with suitable initial conditions and control variables. The well-posedness and numerical analysis of this equation forms a research topic in

itself [5, 7, 16, 18–21], since the entropy solution concept for this model does not emerge as a straightforward limit case of the theory a conservation law with smoothly varying coefficients [25], at least unless one imposes further conditions on the relative sizes of the flux smoothing and the parabolic regularization of the vanishing viscosity method (cf., e.g., [8, 15, 17]).

Typically, many input parameters cannot be described with deterministic accuracy but behave stochastically. In the applications the uncertainty comes, for instance, from the fact that the feed flow comes from other units that are not under control of the CT operator, or from the unpredictability of weather conditions. While a rigorous treatment should take into account two stochastic dimensions, namely the uncertainties of the rate of inflow Q_{F} of feed suspension and that of the solids volume fraction of the feed u_{F}, we will for simplicity only include that of u_{F}. This uncertainty produces a first-order scalar conservation law with a random flux function.
It is the purpose of this work to provide a new efficient method for evaluating the uncertainty of the response of the system, that is, of the exact or numerical solution of the governing PDE, in terms of the uncertainty in the control parameter u_{F}. As a by now classical approach in uncertainty quantification one could apply the stochastic Galerkin method where the random field is represented in terms of orthonormal polynomials. This leads to a very accurate approximation in form of a strongly coupled high-dimensional deterministic system for a finite number of moments [32]. On theother hand one might apply the multi-wavelet stochastic discretization as e.g. in [36]. The approach still leads to a full coupling of the polynomial basis is defined on the whole stochastic domain. The novelty of our approach consists in the application of a hybrid stochastic Galerkin (HSG) method that combines polynomial chaos and multi-wavelet representation. However each stochastic element is equipped with its own polynomial basis. Due this combination the HSG method leads to a partially decoupled deterministic system, that allows *efficient parallelisation*. Furthermore we improve the efficiency of the HSG method by a *adaptive multiresolution concept* in the stochastic space (see also [36] for an adaptive approach in the framework of multi-resolution techniques). The HSG method provides two kinds of adaptivity in the stochastic space: the simple polynomial order truncation and more sophisticated order of resolution adaptivity. While the adaptive parallel HSG methods gives good numerical results for the CT operator it must be pointed out that the overall approach can be applied to a wide range of conservation laws with uncertain coefficients.

1.2 Outline of the paper

The remainder of the paper is organized as follows. In Section 2 the governing models are described. To this end we introduce in Section 2.1 a spatially two-dimensional deterministic model, Model 2D, from which a one-dimensional version, Model 1D, is obtained if we assume that all flow variables depend on depth only. In Section 2.2 we state the final form of both models, including the random feed.
In Sect. 3 we detail the model and introduce an approximation for the random feed u_{F} by a stochastic Galerkin (SG) and the new hybrid stochastic Galerkin ansatz. More specifically we review the polynomial chaos approach in Section 3.1 and define in Section 3.2 the stochastic Galerkin system. This leads after finite volume discretization in the one- and twodimensional physical space to the stochastic Galerkin finite volume method (SG-FV). In Section 3.3 we extend the SG stochastic discretisation to the hybrid stochastic Galerkin (HSG) approach. Next, in Section 3.3.2 we formulate a stochastic Galerkin approach, which makes explicit how the coefficients of the HSG representation are calculated. A fully discrete finite volume formulation for the stochastic Galerkin approaches, namely the respective "HSG–systems", of Model 1D and 2D is introduced in Sections 3.3.3 and 3.3.4 (HSG-FV). In Sect. 3.4 we consider the application of the FV methods introduced in Sections 3.3.3 and 3.3.4 to Models 1D and 2D. We start with experiments in one space dimension and compare the HSG-FV results with those of the Monte Carlo approach. In the two-dimensional case we compare our HSG results with the results of the finest possible stochastic resolution. Note that the computational effort prevents any use of the Monte Carlo approach in this situation! In Sect. 3.5 we discuss the benefits of the parallel application for SG and HSG methods.
The further improvement of the method is stochastic adaptivity (denoted as HSG–adapt), which is introduced in Section 4. The HSG-adapt method reduces the stochastic dimension and increases the computational efficiency decisively.

2 Governing models

2.1 Deterministic versions

The fundamental conservation equations are the continuity equations of the solid and the fluid, which are both considered as continuous, superimposed phases. In differential form, and considering a spatial domain $\tilde{D} \subset \mathbb{R}^d$, $d = 1, 2, 3$, these equations are given by

$$u_t(\mathbf{x}, t) + \operatorname{div}\big(u(\mathbf{x}, t)\mathbf{v}_{\mathrm{s}}\big) = 0, \quad \big(1 - u(\mathbf{x}, t)\big)_t + \operatorname{div}\big((1 - u(\mathbf{x}, t))\mathbf{v}_{\mathrm{s}}\big) = 0, \quad \mathbf{x} \in \tilde{D}, \quad t > 0, \tag{1}$$

where $\mathbf{v}_\mathrm{s}$ and $\mathbf{v}_\mathrm{f}$ are the solid and fluid phase velocities, respectively. If we define the solid-fluid relative velocity $\mathbf{v}_\mathrm{r} := \mathbf{v}_\mathrm{s} - \mathbf{v}_\mathrm{f}$ and the volume-average velocity of the mixture $\mathbf{q} := u\mathbf{v}_\mathrm{s} + (1-u)\mathbf{v}_\mathrm{f}$, then the governing equations (1) can be written as follows, where for the moment we omit the argument "$(\mathbf{x}, t)$":

$$u_t + \operatorname{div}\big(u\mathbf{q} + u(1-u)\mathbf{v}_\mathrm{r}\big) = 0, \quad \operatorname{div}\mathbf{q} = 0, \quad \mathbf{x} \in \tilde{D}, \quad t > 0. \tag{2}$$

For gravity separation, and following a well-known kinematic theory of sedimentation (see [5, 27]), we introduce the constitutive assumption

$$\mathbf{v}_\mathrm{r} = \mathbf{v}_\mathrm{r}(u) = \frac{b(u)}{u(1-u)}\mathbf{e}_x,$$

where $\mathbf{e}_x$ is the unit vector pointing into the direction of gravity and $b = b(u)$ is the so-called Kynch batch flux density function that is frequently given by the Richardson-Zaki expression [34]

$$b(u) = b^{\mathrm{RZ}}(u) := \tilde{b}(u) = \begin{cases} u_\infty u(1-u)^{n_\mathrm{RZ}} & \text{for } 0 \le u \le u_{\max}, \\ 0 & \text{for } u < 0 \text{ and } u > u_{\max}, \end{cases} \tag{3}$$

where $u_\infty > 0$ is the Stokes velocity, that is, the settling velocity of single particle in an unbounded fluid, $0 < u_{\max} \le 1$ is a maximum solids concentration, and $n_\mathrm{RZ} \ge 1$ is a parameter. Thus, if we define the flux vector

$$\tilde{\mathbf{h}}(\mathbf{x}, t, u) := \mathbf{q}(\mathbf{x}, t)u + b\big(u(\mathbf{x}, t)\big)\mathbf{e}_x, \tag{4}$$

then the governing equations (2) reduce to

$$u_t + \operatorname{div}\tilde{\mathbf{h}}(\mathbf{x}, t, u) = 0, \quad \operatorname{div}\mathbf{q} = 0, \quad \mathbf{x} \in \tilde{D}, \quad t > 0, \tag{5}$$

in the absence of sources and sinks. Obviously, only in $d = 1$ dimensions are the two scalar equations (5) solvable for u and $q = \mathbf{q}$. In $d \ge 2$ dimensions an additional equation of motion must be solved; for example, in [11, 12], (5) is solved along with the equation

$$-\operatorname{div}\big(\mu(u)\nabla\mathbf{q}\big) + \lambda\nabla p = -\lambda u g \mathbf{e}_x, \tag{6}$$

where $\mu = \mu(u)$ is a strictly positive viscosity function, $\lambda > 0$ is a constant, $p = p(\mathbf{x}, t)$ is pressure, and g is the acceleration of gravity, i.e. the second equation of (5) and (6) form a version of the Stokes system. (One could also consider the Navier-Stokes equation instead of (6).) In the multi-dimensional setting, the right-hand side of (6) describes the coupling between the concentration and velocity fields. The coupled system (5), (6) is solved (in slight variants) in [11, 12] by finite volume and finite volume element techniques, respectively.

In the present work we wish to partially address the multi-dimensional case, but prefer not to solve the full coupled system (5), (6) for reasons of the considerable additional computational effort, and to avoid that the uncertainty in the concentration field be introduced into the flow field. For this reason we introduce Model 2D and Model 1D (referring to two and one space dimensions, respectively) as follows.

For Model 2D we consider the longitudinal-infinite vessel $D := \mathbb{R} \times S \subset \mathbb{R}^3$ with the cross-sectional domain $S \subset \mathbb{R}^2$ and coordinates $\mathbf{x} = (x_1, x_2, x_3)^\mathrm{T}$. We assume that all flow variables depend on x_1 and x_2 only, and will henceforth write $\mathbf{x} = (x, y)$. Conceptually, this assumption corresponds to a vertical channel of infinite (horizontal) depth, or to an axisymmetric three-dimensional vessel for which the variables depend on the radial and axial coordinates only.

The longitudinal x-direction is aligned with gravity. We assume that at $x_1 = 0$, a singular feed source is located, and that the unit is fed with feed suspension at a volumetric rate $Q_\mathrm{F} = Q_\mathrm{F}(t) \ge 0$ and a feed volume fraction $u_\mathrm{F} = u_\mathrm{F}(t)$. The feed mechanism causes the separation of the feed flow into upward- and downward-directed bulk flows. In fact, we assume that $\mathbf{q} = \mathbf{q}(\mathbf{x}, t) = (q^x(\mathbf{x}, t), q^y(\mathbf{x}, t))$ satisfies

$$\mathbf{q}(\mathbf{x}, t) = \begin{cases} \mathbf{q}_\mathrm{L}(\mathbf{x}, t) & \text{for } x < 0, \\ \mathbf{q}_\mathrm{R}(\mathbf{x}, t) & \text{for } x > 0, \end{cases} \quad \mathbf{q}_\mathrm{L} = (q^x_\mathrm{L}, q^y_\mathrm{L}) \quad \text{and} \quad \mathbf{q}_\mathrm{R} = (q^x_\mathrm{R}, q^y_\mathrm{R}). \tag{7}$$

To ensure global conservativity, we choose $Q_\mathrm{F}(t) = (q^x_\mathrm{R} - q^x_\mathrm{L})S(x = 0)$. In Section A we will construct a flow field that satisfies $\operatorname{div}\mathbf{q} = 0$ along with these conditions and zero-flux boundary conditions, so in the present work $\mathbf{q} = \mathbf{q}(\mathbf{x}, t)$ is given externally. Moreover, it is assumed that the solid-liquid separation takes place within the unit only, identified by the x-interval $(-1, 1)$, while outside both phases move at the same velocity, i.e., $\mathbf{v}_\mathrm{r} = 0$. Thus, instead of the flux given by (4)

we employ the nonlinear flux $\mathbf{h}(\mathbf{x},t,u) = u(\mathbf{x},t)\boldsymbol{\gamma}^1(\mathbf{x},t) + \gamma^2(\mathbf{x})b(u)$, where we define the discontinuous (with respect to x) parameters

$$\boldsymbol{\gamma}^1(\mathbf{x},t) := \begin{cases} \mathbf{q}_{\mathrm{L}}(\mathbf{x},t) & \text{for } x < 0, \\ \mathbf{q}_{\mathrm{R}}(\mathbf{x},t) & \text{for } x > 0, \end{cases} \qquad \gamma^2(\mathbf{x}) := \begin{cases} 1 & \text{for } x \in (-1,1), \\ 0 & \text{for } x \notin (-1,1). \end{cases}$$

Modelling the solids feed mechanism by a singular source term we obtain the following governing equation for Model 2D:

$$u_t(\mathbf{x},t) + \operatorname{div}\big(\mathbf{h}(\mathbf{x},t,u(\mathbf{x},t))\big) = \delta(x)Q_{\mathrm{F}}(t)u_{\mathrm{F}}(t) \quad \text{on } D_T \times \Omega, \tag{8}$$

which is solved along with the initial condition $u(\mathbf{x},0) = u_0(\mathbf{x})$ for $\mathbf{x} \in D$, and where $\mathbf{q} = \mathbf{q}(\mathbf{x},t)$ is given externally such that $\operatorname{div}\mathbf{q} = 0$ and (7) is satisfied.

The uncertainty in u_{F} and the final form of this model and Model 1D will be introduced in Section 2.2. Model 1D is the spatially one-dimensional version of Model 2D obtained under the assumption that all flow variables depend on depth x only. It arises from the assumption that the cross section of the unit, corresponding to the x-interval, is constant. If uncertainty is not built in, then Model 1D is equivalent to the one-dimensional clarifier-thickener models studied in [5, 6]. The governing initial value problem is then

$$\begin{aligned} u_t(x,t) + \big(h(x,t,u(x,t))\big)_x &= \delta(x)Q_{\mathrm{F}}(t)u_{\mathrm{F}}(t) \quad \text{on } \Pi_T := \mathbb{R}\times(0,T), \\ u(x,0) &= u_0(x), \quad x \in \mathbb{R}. \end{aligned}$$

2.2 Random feed and final formulation of models 2D and 1D

In this work we assume that the feed concentration u_{F} exhibits stochastic variability. In fact, for the probability measure P let $\Omega = (\Omega, P)$ be the probability space, and we denote the random feed volume fraction by $u_{\mathrm{F}} = u_{\mathrm{F}}(\omega) \in [0,1]$, where $\omega \in \Omega$. For both models it is assumed that the feed source is distributed over the whole cross section $\{0\} \times S$. As we will show below, the complete feed term in (8) can be rewritten as part of the flux such that (8) assumes the form of a nonlinear conservation law with discontinuous flux. To our knowledge, such a situation has not yet been treated in the framework of uncertainty quantification. For Model 2D we may rewrite the source term as a part of the convective flux via

$$\delta(x)Q_{\mathrm{F}}(t)u_{\mathrm{F}}(t,\omega) = \operatorname{div}\big(H(x)Q_{\mathrm{F}}(t)u_{\mathrm{F}}(t,\omega)\mathbf{e}_x\big),$$

where H denotes the Heaviside function and $\mathbf{e}_x$ is the unit vector pointing into the x-direction. For Model 1D we obtain the simpler expression

$$\delta(x)Q_{\mathrm{F}}(t)u_{\mathrm{F}}(t,\omega) = \big(H(x)Q_{\mathrm{F}}(t)u_{\mathrm{F}}(t,\omega)\big)_x.$$

Thus, Model 2D can finally be cast into the following form: for a final time $T > 0$ we seek the solids volume fraction $u : D_T := D \times (0,T) \to [0,1]$ as the solution of the initial value problem

$$\begin{aligned} u_t(\mathbf{x},t,\omega) + \operatorname{div}\mathbf{g}(\mathbf{x},t,u,\omega) &= 0 \quad \text{in } D_T \times (0,T) \times \Omega, \\ u(\mathbf{x},0,\omega) &= u_0(\mathbf{x}), \quad \mathbf{x} \in D, \end{aligned} \tag{9}$$

where the flux function $\mathbf{g}$ is determined for $t \in (0,T)$ and $\omega \in \Omega$ by

$$\mathbf{g}(\mathbf{x},t,u,\omega) = \mathbf{h}(\mathbf{x},t,u) - H(x)Q_{\mathrm{F}}(t)u_{\mathrm{F}}(t,\omega)\mathbf{e}_x,$$

which for Model 1D reduces to

$$g(x,t,u,\omega) = h(x,t,u) - H(x)Q_{\mathrm{F}}(t)u_{\mathrm{F}}(t,\omega).$$

Thus, the flux vector for Model 2D is given by

$$\mathbf{g}(\mathbf{x},t,u,\omega) = \begin{cases} (u - u_{\mathrm{F}}(t,\omega))\mathbf{q}_{\mathrm{L}}(\mathbf{x},t) & \text{for } x < -1, \\ (u - u_{\mathrm{F}}(t,\omega))\mathbf{q}_{\mathrm{L}}(\mathbf{x},t) + b(u)\mathbf{e}_x & \text{for } -1 < x < 0, \\ (u - u_{\mathrm{F}}(t,\omega))\mathbf{q}_{\mathrm{R}}(\mathbf{x},t) + b(u)\mathbf{e}_x & \text{for } 0 < x < 1, \\ (u - u_{\mathrm{F}}(t,\omega))\mathbf{q}_{\mathrm{R}}(\mathbf{x},t) & \text{for } x > 1, \end{cases} \tag{10}$$

with an obvious analogous expression (not written out here) for the flux $g = g(x, t, u, \omega)$ of Model 1D.

The flux (10) has discontinuities for $x \in \{-1, 0, 1\}$. We will not directly work with (9) and the flux defined by (10) but expand the PDE (9) into a system. To this end, we define the flux vector

$$\mathbf{f}(t, u, \boldsymbol{\gamma}^1, \boldsymbol{\gamma}^2, \omega) := \big(u - u_{\mathrm{F}}(t, \omega)\big)\boldsymbol{\gamma}^1 + b(u)\gamma^2 \mathbf{e}_x,$$

where the unknown vector is now $(u, \boldsymbol{\gamma}^1, \gamma^2)^{\mathrm{T}} \in \mathbb{R}^2 \times \mathbb{R}$. This vector is solution to the system of balance laws

$$\begin{aligned} u(\mathbf{x}, t, \omega)_t + \operatorname{div}\big(f(t, u, \boldsymbol{\gamma}^1, \gamma^2, \omega)\big) &= 0, \\ \boldsymbol{\gamma}^1_t(\mathbf{x}, t) &= H(x)\big(\mathbf{q}_{\mathrm{R}}(\mathbf{x}, t) + H(-x)\mathbf{q}_{\mathrm{L}}(\mathbf{x}, t)\big)_t, \\ \gamma^2_t(\mathbf{x}, t) &= 0, \end{aligned} \tag{11}$$

subject to the initial conditions

$$\begin{aligned} u(\mathbf{x}, 0, \omega) &= u_0(\mathbf{x}), \\ \boldsymbol{\gamma}^1(\mathbf{x}, 0) &= H(x)\mathbf{q}_{\mathrm{R}}(\mathbf{x}, 0) + H(-x)\mathbf{q}_{\mathrm{L}}(\mathbf{x}, 0), \\ \gamma^2(\mathbf{x}) &= \chi_{(-1,1)}(x). \end{aligned}$$

3 A hybrid stochastic Galerkin (HSG) finite volume method

In this section we start with a polynomial chaos (PC) method and its application to the governing equation (11). In Section 3.3 we extend the PC stochastic discretization to the hybrid stochastic Galerkin (HSG) method and discuss its application to the governing model.

3.1 Preliminaries and polynomial chaos

Let $\theta = \theta(\omega)$ be a random variable on the probability space (Ω, P) which satisfies $\theta \in L^2(\Omega)$. We assume that the distribution of θ is known and that the probability density function ρ is given. The expectation of θ is given by

$$\mathbb{E}[\theta] := \int_\Omega \theta(\omega)\,\mathrm{d}P(\omega) = \int_\Omega \theta\,\mathrm{d}\rho(\theta).$$

Let $\{\phi_p(\theta)\}_{p\in\mathbb{N}_0}$ be a family of $L^2(\Omega)$-orthonormal polynomials with respect to the probability density function ρ. This means that $\{\phi_p(\theta)\}_{p\in\mathbb{N}_0}$ satisfies

$$\langle \phi_p(\theta),\, \phi_q(\theta)\rangle_{L^2(\Omega)} := \int_\Omega \phi_p\big(\theta(\omega)\big)\,\phi_q\big(\theta(\omega)\big)\,\mathrm{d}P(\omega) = \delta_{p,q} \quad \text{for } p, q \in \mathbb{N}_0. \tag{12}$$

Here $\delta_{p,q}$ denotes the Kronecker symbol. The choice of the polynomials ϕ_p depends on the probability density function ρ. For example, Gauss distribution requires Hermite polynomials, and Legendre polynomials allow us to use the approach of uniformly distributed random variables. For definitions of the polynomials cf. [31].

The random field $w = w(\mathbf{x}, t, \omega) = w(\mathbf{x}, t, \theta(\omega))$, $(\mathbf{x}, t) \in D_T$, with finite variance can be represented by the infinite series

$$w\big(\mathbf{x}, t, \theta(\omega)\big) = \sum_{p=0}^{\infty} w^p(\mathbf{x}, t)\phi_p\big(\theta(\omega)\big), \quad (\mathbf{x}, t) \in D_T.$$

Here the coefficients $w^p = w^p(\mathbf{x}, t)$, $(\mathbf{x}, t) \in D_T$ are defined by

$$w^p := \langle w,\, \phi_p\rangle_{L^2(\Omega)} = \int_\Omega w\big(\theta(\omega)\big)\phi_p\big(\theta(\omega)\big)\,\mathrm{d}P(\omega) \;\text{ for } p \in \mathbb{N}_0.$$

Note that the expectation of the random field w is given by the coefficient w^0 and its variance is given by the series $\sum_{p=1}^{\infty}(w^p)^2$. The truncation at the highest polynomial order $N_{\mathrm{o}} \in \mathbb{N}$ yields a finite sum, namely

$$\Pi^{N_{\mathrm{o}}}[w]\big(\mathbf{x}, t, \theta(\omega)\big) := \sum_{p=0}^{N_{\mathrm{o}}} w^p(\mathbf{x}, t)\phi_p\big(\theta(\omega)\big), \quad (\mathbf{x}, t) \in D_T. \tag{13}$$

The Cameron-Martin Theorem in [14, 39] ensures convergence of the series in (13), i.e., $\Pi^{N_{\mathrm{o}}}[w] \to w$ in $L^2(\Omega)$ for $N_{\mathrm{o}} \to \infty$. For further reading we refer to [23, 29, 32].

3.2 The stochastic Galerkin finite volume (SG-FV) method

Similarly to [33] we apply the PC framework to the governing model. The resulting weakly hyperbolic system allows us to use appropriate finite volume methods in one and two space dimensions.

3.2.1 Formulation of the stochastic Galerkin system

Let us again consider the governing equation (11). We test the equation with $\phi_0, \dots, \phi_{N_\mathrm{o}}$ and obtain the system

$$\int_\Omega \big(u_t(\mathbf{x},t,\theta(\omega)) + \operatorname{div}\Big(\big(u(\mathbf{x},t,\theta(\omega)) - u_\mathrm{F}(t,\theta(\omega))\big)\mathbf{q}(\mathbf{x},t) + \gamma^2(\mathbf{x}) b\big(u(\mathbf{x},t,\theta(\omega))\big)\mathbf{e}_x\Big)\Big)\phi_p(\theta(\omega))\,\mathrm{d}P(\omega) = 0 \quad \text{for } p = 0,\dots,N_\mathrm{o}.$$

We replace $u(\mathbf{x},t,\omega)$ by the truncated PC-expansion

$$\Pi^{N_\mathrm{o}}[u](\mathbf{x},t,\theta(\omega)) = \sum_{p=0}^{N_\mathrm{o}} u^p(\mathbf{x},t)\phi_p\big(\theta(\omega)\big).$$

Using now the orthogonality relation (12) we obtain the truncated **SG system** for the coefficients $u^0,\dots,u^{N_\mathrm{o}}$

$$u_t^k + \operatorname{div}\left(\left(u^k - u_\mathrm{F}^k\right)\mathbf{q} + \gamma^2 \left\langle b\left(\sum_{p=0}^{N_\mathrm{o}} u^p\phi_p\right)\mathbf{e}_x,\ \phi_0\right\rangle_{L^2(\Omega)}\right) = 0, \quad k = 0,\dots,N_\mathrm{o}. \tag{14}$$

We get finally from (14) and the equations for $\mathbf{q}$ and γ^2 an $(N_\mathrm{o}+3)$-dimensional system. It can be shown that this system is weakly hyperbolic (cf. [38]).

Remark 3.1

1. The approximate solution $\Pi^{N_\mathrm{o}}[u]$ allows us to compute easily stochastic quantities like expectation or variance from the coefficients $u^0,\dots,u^{N_\mathrm{o}}$. Consequently, it is not necessary to compute the required stochastic quantities during the computation or to store data for each realization as in Monte-Carlo simulations.
2. The structure of the system (14) makes a parallel computation in the stochastic dimensional complicated. Due to the nonlinear flux and coupled representation of $u(\mathbf{x},t,\omega)$ the computation requires synchronisation in each time-step which makes sense only on shared-memory machines and for small numbers of N_o.

3.2.2 1D finite volume method

The system (14) is quite general and it appears hard to construct e.g. a Godunov-type solver without further analytical knowledge. Furthermore the common upwind-biased Engquist-Osher flux [22], which is usually applied for scalar problems with discontinuous flux [5–7], cannot be used for the higher-dimensional SG-system (14). Therefore, at least for the computations in one space dimension, as in [33], we use the simple Lax-Friedrichs method on a uniform mesh with cells $[x_{i-1/2}, x_{i+1/2})$, $i \in \mathbb{Z}$ and $\Delta x = x_{i+1/2} - x_{i-1/2}$. Restricting to the u-components $u^0,\dots,u^{N_\mathrm{o}}$ we have for time step $\Delta t^n > 0$ the **SG-FV scheme**

$$u_i^{p,n+1} = u_i^{p,n} - \frac{\Delta t^n}{\Delta x}\left(F_{i+1/2}^{p,n} - F_{i-1/2}^{p,n}\right) \qquad (i\in\mathbb{Z},\ n\in\mathbb{N},\ p=0,\dots,N_\mathrm{o}),$$

$$F_{i+1/2}^{p,n} := \frac{1}{2}\Bigg(f^p\left(t^n, u_i^{0,n},\dots,u_i^{N_\mathrm{o},n},(\gamma^1)_i^n,(\gamma^2)_i^n\right) + f^p\left(t^n, u_{i+1}^{0,n},\dots,u_{i+1}^{N_\mathrm{o},n},(\gamma^1)_{i+1}^n,(\gamma^2)_{i+1}^n\right)\Bigg) + \frac{\Delta x}{2\Delta t^n}\left(u_{i+1}^{p,n} - u_i^{p,n}\right).$$

The function f^p, for $p = 0,\dots,N_\mathrm{o}$ is defined by

$$f^p\left(t,u^0,\dots,u^{N_\mathrm{o}},\gamma^1,\gamma^2\right) = \gamma^1\left(u^p - u_\mathrm{F}^p\right) + \gamma^2\left\langle b\left(\sum_{q=0}^{N_\mathrm{o}} u^q\phi_q\right),\ \phi_p\right\rangle_{L^2(\Omega)}.$$

Initial values are obtained from $u_i^{0,0} = u_0$ and $u_i^{1,0} = \ldots = u_i^{N_\mathrm{o},0} = 0$ (cf. (9)).

3.2.3 2D finite volume method

As in the 1D case we consider the $(N_\mathrm{o}+3)$-dimensional system (14) in 2D. The flux function is given by $F = (F^0, \dots, F^{N_\mathrm{o}})^\mathrm{T}$, where F^p for $p = 0, \dots, N_\mathrm{o}$ is defined by

$$F^p(u, \mathbf{q}, \gamma^2, x, y, t) := (u^p - (u_\mathrm{F})^p(t))\, \mathbf{q} + \gamma^2 \left\langle b \left(\sum_{q=0}^{N_\mathrm{o}} u^q \phi_q \right) \mathbf{e}_x,\ \phi_p \right\rangle_{L^2(\Omega)}.$$

For the computation we use the central-upwind numerical scheme by Kurganov and Petrova [26] on the triangulation $\mathcal{T} := \bigcup\{T_j\}$ consisting of triangular cells T_j. The semi-discrete **SG-FV scheme** is given by

$$\frac{d}{dt}\bar{\mathbf{u}}_j := -\frac{1}{|T_j|} \sum_{k=1}^{3} h_{jk} \left(\frac{a_{jk}^{\mathrm{in}} F(\tilde{\mathbf{u}}_{jk}, \mathbf{q}, \gamma^2, M_j(k), t) + a_{jk}^{\mathrm{out}} F(\tilde{\mathbf{u}}_j, \mathbf{q}, \gamma^2, M_j(k))}{a_{jk}^{\mathrm{in}} + a_{jk}^{\mathrm{out}}} \right) \cdot \mathbf{n}_{jk} + \frac{1}{|T_j|} \sum_{k=1}^{3} h_{jk} \frac{a_{jk}^{\mathrm{in}} a_{jk}^{\mathrm{out}}}{a_{jk}^{\mathrm{in}} + a_{jk}^{\mathrm{out}}} \left[\tilde{\mathbf{u}}_{jk}(M_j(k)) - \tilde{\mathbf{u}}_j(M_j(k)) \right].$$

Here the $N_\mathrm{o}+1$-dimensional vector $\bar{\mathbf{u}}_j$ is the cell average on the triangle T_j, h_{jk} is the length of the k-th side, $k = 1, 2, 3$, the point $M_j(k)$ is the midpoint of the k-th side, n_{jk} is the outer normal on the k-th side, a_{jk}^{in} and a_{jk}^{out} are directional local speeds on the k-th side. The central-upwind numerical scheme uses reconstruction $\tilde{\mathbf{u}}$ and $\tilde{\mathbf{u}}_j(G)$ and $\tilde{\mathbf{u}}_{jk}(G)$ denotes admissible reconstructions on the point G over the cells T_j and T_{jk} respectively (see [26] for the details). Note that the SG-FV approach as in 1D requires no specific information as e.g Godunov solver.

For the computation of the eigenvalues Jacobian matrix we use LAPACK [4]. The initial Delaunay triangulation is generated by Triangle [35]. The implementation uses adaptive mesh refinement.

3.3 A hybrid stochastic Galerkin (HSG) finite volume method

The SG-FV method permits fast and accurate computations for a small maximal polynomial order N_o. Increasing the polynomial order N_o will significantly increase the computational effort and the synchronisation costs. The hybrid stochastic Galerkin (HSG) method, that is introduced in this section allows us to reduce the maximal polynomial order N_o and to obtain a partially decoupled system of equations. This reduces the synchronisation effort of the parallel computation significantly and permits efficient parallel computing on distributed memory machines.

3.3.1 Stochastic discretization

Let $\theta = \theta(\omega)$ be again a random variable on the probability space (Ω, P) which satisfies $\theta \in L^2(\Omega)$. For sake of brevity we assume that θ is uniformly distributed on the interval $[0, 1]$. The main idea of the method introduced is the dyadical decomposition of the stochastic domain $[0, 1]$.

For $N_\mathrm{o} \in \mathbb{N}_0$ and $N_\mathrm{r} \in \mathbb{N}_0$ we define the interval $I_l^{N_\mathrm{r}} := [2^{-N_\mathrm{r}} l, 2^{-N_\mathrm{r}}(l+1)]$, and the following space of piecewise continuous polynomials $S^{N_\mathrm{o},\, N_\mathrm{r}}$:

$$S^{N_\mathrm{o},\, N_\mathrm{r}} := \left\{ w : [0,1] \to \mathbb{R} \;\middle|\; w|_{I_l^{N_\mathrm{r}}} \in \mathbb{Q}_{N_\mathrm{o}}[\theta],\ \forall\, l \in \{0, \dots, 2^{N_\mathrm{r}} - 1\} \right\}. \tag{15}$$

Here $\mathbb{Q}_{N_\mathrm{o}}[\theta]$ denotes the space of real polynomials with degree $\leq N_\mathrm{o}$. The vector space $S^{N_\mathrm{o},\, N_\mathrm{r}}$ has the dimension $2^{N_\mathrm{r}}(N_\mathrm{o}+1)$. Note that the vector space $S^{N_\mathrm{o},\, 0}$ corresponds to the PC approach introduced in Section 3.1. The basis of $S^{N_\mathrm{o},\, 0}$ can be given by rescaled Legendre polynomials ϕ_p, $p = 0, \dots, N_\mathrm{o}$, such that

$$\langle \phi_p(\theta(\omega)),\, \phi_q(\theta(\omega)) \rangle_{L^2(\Omega)} = \delta_{p,q} \quad \text{for } 0 \leq p, q \leq N_\mathrm{o}. \tag{16}$$

The space $S^{N_\mathrm{o},\, N_\mathrm{r}}$ is spanned by the polynomials $\phi_{p,l}^{N_\mathrm{r}}$ defined by

$$\phi_{p,l}^{N_\mathrm{r}}(\xi) = \begin{cases} 2^{N_\mathrm{r}/2} \phi_p(2^{N_\mathrm{r}} \xi - l) & \text{for } \xi \in I_l^{N_\mathrm{r}}, \\ 0 & \text{otherwise} \end{cases} \quad \text{for } p = 0, \dots, N_\mathrm{o} \text{ and } l = 0, \dots, 2^{N_\mathrm{r}} - 1.$$

The polynomials $\phi_{p,l}^{N_\mathrm{r}}$ satisfy the orthogonality relation

$$\left\langle \phi_{p,l}^{N_\mathrm{r}}(\theta(\omega)),\, \phi_{q,k}^{N_\mathrm{r}}(\theta(\omega)) \right\rangle_{L^2(\Omega)} = \delta_{p,q}\delta_{k,l} \quad \text{for } 0 \leq p, q \leq N_\mathrm{o} \text{ and } 0 \leq k, l \leq 2^{N_\mathrm{r}} - 1.$$

Let w be a random field that satisfies $w(\mathbf{x},t,\theta(\cdot)) \in L^2(\Omega)$, $\mathbf{x} \in D_T$, $t \in [0,T]$. The projection $\Pi^{N_\mathrm{o},N_\mathrm{r}} : L^2(\Omega) \to S^{N_\mathrm{o},N_\mathrm{r}}$ is defined by

$$\Pi^{N_\mathrm{o},N_\mathrm{r}}[w](\mathbf{x},t,\theta) := \sum_{l=0}^{2^{N_\mathrm{r}}-1}\sum_{p=0}^{N_\mathrm{o}} \left\langle w(\mathbf{x},t,\theta),\, \phi_{p,l}^{N_\mathrm{r}}\right\rangle_{L^2(\Omega)} \phi_{p,l}^{N_\mathrm{r}}(\theta) := \sum_{l=0}^{2^{N_\mathrm{r}}-1}\sum_{p=0}^{N_\mathrm{o}} w_{p,l}^{N_\mathrm{r}}(\mathbf{x},t)\phi_{p,l}^{N_\mathrm{r}}(\theta).$$

Here the coefficients $w_{p,l}^{N_\mathrm{r}}$ are given by

$$w_{p,l}^{N_\mathrm{r}} := \left\langle w,\, \phi_{p,l}^{N_\mathrm{r}}\right\rangle_{L^2(\Omega)} \quad \text{for } 0 \le p \le N_\mathrm{o} \text{ and } 0 \le l \le 2^{N_\mathrm{r}}-1.$$

For the approximation property of the projection $\Pi^{N_\mathrm{o},N_\mathrm{r}}$ for $N_\mathrm{o},\, N_\mathrm{r} \to \infty$ we refer to [3]. The expectation and variance of the projection $\Pi^{N_\mathrm{o},N_\mathrm{r}}[w]$ can be directly computed through the following respective formulas:

$$\begin{aligned}
\mathbb{E}\left[\Pi^{N_\mathrm{o},N_\mathrm{r}}[w](\mathbf{x},t)\right] &:= \sum_{l=0}^{2^{N_\mathrm{r}}-1}\sum_{p=0}^{N_\mathrm{o}} w_{p,l}^{N_\mathrm{r}}(\mathbf{x},t)\left\langle \phi_{p,l}^{N_\mathrm{r}},\, \phi_{0,0}^{0}\right\rangle_{L^2(\Omega)},\\
\mathrm{Var}\left[\Pi^{N_\mathrm{o},N_\mathrm{r}}[w](\mathbf{x},t)\right] &:= \sum_{l=0}^{2^{N_\mathrm{r}}-1}\sum_{p=0}^{N_\mathrm{o}}\sum_{q=0}^{N_\mathrm{o}} w_{p,l}^{N_\mathrm{r}}(\mathbf{x},t)w_{q,l}^{N_\mathrm{r}}(\mathbf{x},t)\left\langle \phi_{p,l}^{N_\mathrm{r}}\phi_{q,l}^{N_\mathrm{r}},\, \phi_{0,0}^{0}\right\rangle_{L^2(\Omega)}\\
&\quad - \left(\mathbb{E}\left[\Pi^{N_\mathrm{o},N_\mathrm{r}}[w](\mathbf{x},t)\right]\right)^2,
\end{aligned}$$

In the case that the random field w is uniformly distributed on the interval $[0,1]$, usually denoted by $w \sim \mathcal{U}(0,1)$, we have $\phi_{0,0}^0 \equiv 1$. Together with the orthogonality of $\phi_{q,l}^{N_\mathrm{r}}$, $q = 0,\dots,N_\mathrm{o}$, $l = 0,\dots,2^{N_\mathrm{r}}-1$ this implies

$$\mathrm{Var}\left[\Pi^{N_\mathrm{o},N_\mathrm{r}}[w](\mathbf{x},t)\right] := \sum_{l=0}^{2^{N_\mathrm{r}}-1}\sum_{p=0}^{N_\mathrm{o}}\left(w_{p,l}^{N_\mathrm{r}}(\mathbf{x},t)\right)^2 - \left(\mathbb{E}\left[\Pi^{N_\mathrm{o},N_\mathrm{r}}[w](\mathbf{x},t)\right]\right)^2.$$

3.3.2 Application of the hybrid stochastic Galerkin approach to the clarifier-thickener model

Now we can apply the stochastic discretization introduced above to the governing equation (11). The idea behind this method is to replace the stochastically perturbed parameter u_F and the unknown solution u by their respective projections onto $S^{N_\mathrm{r},N_\mathrm{o}}$, denoted by $\Pi^{N_\mathrm{o},N_\mathrm{r}}[u_\mathrm{F}]$ and $\Pi^{N_\mathrm{o},N_\mathrm{r}}[u]$, respectively, and to compute the coefficients $u_{0,0}^{N_\mathrm{r}},\dots,u_{N_\mathrm{o},2^{N_\mathrm{r}}-1}^{N_\mathrm{r}}$ of $\Pi^{N_\mathrm{o},N_\mathrm{r}}[u]$. In other words, the **HSG approach** (for the first equation in (11)) reads as follows. For $N_\mathrm{o} \in \mathbb{N}_0$ and $N_\mathrm{r} \in \mathbb{N}_0$, find $u_{0,0}^{N_\mathrm{r}},\dots,u_{N_\mathrm{o},2^{N_\mathrm{r}}-1}^{N_\mathrm{r}} : D_T \to \mathbb{R}$ such that

$$\begin{aligned}
&\int_\Omega \Big(\Pi^{N_\mathrm{o},N_\mathrm{r}}[u]_t + \mathrm{div}\left(\left(\Pi^{N_\mathrm{o},N_\mathrm{r}}[u] - \Pi^{N_\mathrm{o},N_\mathrm{r}}[u_\mathrm{F}]\right)\mathbf{q} + \gamma^2 b\left(\Pi^{N_\mathrm{o},N_\mathrm{r}}[u]\right)\mathbf{e}_x\right)\Big)\phi\,\mathrm{d}P(\omega) = 0,\\
&\text{where}\quad \phi = \phi_{0,0}^{N_\mathrm{r}},\dots,\phi_{N_\mathrm{o},0}^{N_\mathrm{r}},\phi_{0,1}^{N_\mathrm{r}},\dots,\phi_{N_\mathrm{o},2^{N_\mathrm{r}}-1}^{N_\mathrm{r}}.
\end{aligned}$$

Since the support of $\phi_{i,l}^{N_\mathrm{r}}$, $i = 0,\dots,N_\mathrm{o}$, $l = 0,\dots,2^{N_\mathrm{r}}-1$, is given by the stochastic element $I_l^{N_\mathrm{r}}$, the system is decoupled in the stochastic element index l. This property is fundamental for what follows.

Let us replace the inidices $i = 0,\dots,N_\mathrm{o}$ and $l = 0,\dots,2^{N_\mathrm{r}}-1$ by the multi-index $\alpha = (i,l)$, $i = 0,\dots,N_\mathrm{o}$ and $l = 0,\dots,2^{N_\mathrm{r}}-1$ or equivalently, $\alpha = 0,\dots,P = (N_\mathrm{o}+1)2^{N_\mathrm{r}}-1$. Then the system can be compactly written in the following form. For $N_\mathrm{o} \in \mathbb{N}_0$ and $N_\mathrm{r} \in \mathbb{N}_0$ find $u_0^{N_\mathrm{r}},\dots,u_P^{N_\mathrm{r}} : D_T \to \mathbb{R}$ such that

$$\begin{aligned}
&\int_\Omega \Big(\Pi^{N_\mathrm{o},N_\mathrm{r}}[u]_t\\
&\qquad + \mathrm{div}\left(\left(\Pi^{N_\mathrm{o},N_\mathrm{r}}[u] - \Pi^{N_\mathrm{o},N_\mathrm{r}}[u_\mathrm{F}]\right)\mathbf{q} + \gamma^2 b\left(\Pi^{N_\mathrm{o},N_\mathrm{r}}[u]\right)\mathbf{e}_x\right)\Big)\phi_\alpha^{N_\mathrm{r}}\,\mathrm{d}P(\omega) = 0, \quad \alpha = 0,\dots,P.
\end{aligned} \tag{17}$$

For the given stochastically one-dimensional approximation of u_F we employ the notation $\Pi^{N_\mathrm{o},N_\mathrm{r}}[u_\mathrm{F}]$. Using now the orthogonality from (16), we can rewrite (17) in the form

$$u_t^\alpha + \mathrm{div}\left(\left(u^\alpha - (u_\mathrm{F})^\alpha(t)\right)\mathbf{q} + \gamma^2\left\langle b\left(\Pi^{N_\mathrm{o},N_\mathrm{r}}[u]\right)\mathbf{e}_x,\, \phi_\alpha^{N_\mathrm{r}}\right\rangle_{L^2(\Omega)}\right) = 0, \qquad \alpha = 0,\dots,P. \tag{18}$$

In the spatially one-dimensional case, the system (18) can be reduced to the system

$$u_t^\alpha + \left(\gamma^1\left(u^\alpha - (u_\mathrm{F})^\alpha(t)\right) + \gamma^2\left\langle b\left(\Pi^{N_\mathrm{o},N_\mathrm{r}}[u]\right),\, \phi_\alpha^{N_\mathrm{r}}\right\rangle_{L^2(\Omega)}\right)_x = 0, \quad \alpha = 0,\dots,P. \tag{19}$$

With the method introduced in [38] we finally obtain from (18) or (19) a $(P+3)$-dimensional system for the determination of unknown $\mathbf{u}$. Using the (weak) hyperbolicity of (11) and the decoupled structure it can be shown that this system (19) is weakly hyperbolic.

The system (18) is decoupled in the stochastic element index $l = 0, \ldots, 2^{N_\mathrm{r}} - 1$. This allows the efficient parallelisation on the distributed memory machines since the synchronisation between decoupled nodes can be omitted.

3.3.3 1D finite volume method

Similarly to the stochastic Galerkin approach in the Section 3.2.2 we use the Lax-Friedrichs method on a uniform mesh with cells $[x_{i-1/2}, x_{i+1/2})$, $i \in \mathbb{Z}$ and $\Delta x = x_{i+1/2} - x_{i-1/2}$ for the computations in one space dimension. In contrast to scalar problems with discontinuous flux [5–7] the common upwind-biased Engquist-Osher flux [22] cannot be used for the higher–dimensional stochastic Galerkin system. Restricting ourselves to the u-components $u^0, \ldots, u^P$ we have for time step $\Delta t^n > 0$ the **HSG-FV scheme**

$$
\begin{aligned}
u_i^{\alpha,n+1} &= u_i^{\alpha,n} - \frac{\Delta t^n}{\Delta x}\left(F_{i+1/2}^{\alpha,n} - F_{i-1/2}^{\alpha,n}\right) \qquad (i \in \mathbb{Z},\, n \in \mathbb{N},\, \alpha = 0, \ldots, P),\\
F_{i+1/2}^{\alpha,n} &:= \frac{1}{2}\Bigg(f^\alpha\left(t^n, u_i^{0,n}, \ldots, u_i^{P,n}, (\gamma^1)_i^n, (\gamma^2)_i^n\right)\\
&\qquad + f^\alpha\left(t^n, u_{i+1}^{0,n}, \ldots, u_{i+1}^{P,n}, (\gamma^1)_{i+1}^n, (\gamma^2)_{i+1}^n\right)\Bigg) + \frac{\Delta x}{2\Delta t^n}\left(u_{i+1}^{\alpha,n} - u_i^{\alpha,n}\right).
\end{aligned}
$$

The function f^α for $\alpha = 0, \ldots, P$ is defined by

$$
f^\alpha\left(t, u^0, \ldots, u^P, \gamma^1, \gamma^2\right) = \gamma^1\left(u^\alpha - u_\mathrm{F}^\alpha\right) + \gamma^2 \left\langle b\left(\Pi^{N_\mathrm{o}, N_\mathrm{r}}[u]\right),\, \phi_\alpha \right\rangle_{L^2(\Omega)}.
$$

Initial values are obtained from $u_i^{\alpha,0} = u_0 \cdot \left\langle \phi_\alpha^{N_\mathrm{r}},\, \phi_{0,0}^0 \right\rangle_{L^2(\Omega)}$, for $\alpha = 0, \ldots, P$ (cf. (9)).

3.3.4 2D finite volume method

Let us consider the $(P+3)$-dimensional system (18) with flux function given by $F = (F^0, \ldots, F^P)^\mathrm{T}$, where F^α for $\alpha = 0, \ldots, P$ is defined by

$$
F^\alpha(u, \mathbf{q}, \gamma^2, x, y, t) := \left(u^\alpha - (u_\mathrm{F})^\alpha(t)\right)\mathbf{q} + \gamma^2 \left\langle b\left(\Pi^{N_\mathrm{o}, N_\mathrm{r}}[u]\right)\mathbf{e}_x,\, \phi_\alpha^{N_\mathrm{r}} \right\rangle_{L^2(\Omega)}.
$$

For the computation we use again the central-upwind numerical scheme [26] on the triangulation $\mathcal{T} := \bigcup\{T_j\}$ consisting of triangular cells T_j. The semi-discrete **HSG-FV scheme** is given by

$$
\begin{aligned}
\frac{d}{dt}\bar{\mathbf{u}}_j := -\frac{1}{|T_j|}\sum_{k=1}^{3} h_{jk}\left(\frac{a_{jk}^\mathrm{in} F(\tilde{\mathbf{u}}_{jk}, \mathbf{q}, \gamma^2, M_j(k), t) + a_{jk}^\mathrm{out} F(\tilde{\mathbf{u}}_j, \mathbf{q}, \gamma^2, M_j(k))}{a_{jk}^\mathrm{in} + a_{jk}^\mathrm{out}}\right)\cdot \mathbf{n}_{jk}\\
+ \frac{1}{|T_j|}\sum_{k=1}^{3} h_{jk}\frac{a_{jk}^\mathrm{in} a_{jk}^\mathrm{out}}{a_{jk}^\mathrm{in} + a_{jk}^\mathrm{out}}\left[\tilde{\mathbf{u}}_{jk}(M_j(k)) - \tilde{\mathbf{u}}_j(M_j(k))\right].
\end{aligned}
$$

Here $\bar{\mathbf{u}}_j$ is the cell average on the triangle T_j. For $k = 1, 2, 3$ we denote by h_{jk} the length of the k-th edge. The number $M_j(k) \in \mathbb{R}^2$ is the midpoint of the k-th edge and n_{jk} is the outer normal on the k-th edge, a_{jk}^in and a_{jk}^out are the so-called directional local speeds associated with the k-th edge. The central-upwind numerical scheme uses the reconstructions $\tilde{\mathbf{u}}_j$ and $\tilde{\mathbf{u}}_{jk}$(see [26] for the details). The initial Delaunay triangulation is generated by the mesh generator *Triangle* [35]. Note that we use an adaptive dynamic mesh refinement and coarsening which will not be detailed here.

3.4 Numerical experiments

Now we can apply the previously defined hybrid stochastic Galerkin finite volume (HSG-FV) method. Let us start with computations in one space dimension and proceed with the 2D case for some given velocity field. We analyse the accuracy of the method. At least in one space dimension we can compute a sufficiently accurate Monte-Carlo finite volume (MC-FV) numerical solution with a reasonable effort. We use the MC-FV result as the reference solution. In the two dimensional case the computation of the reasonable number of samples is not practicable because of the computational effort. Consequently, in the two-dimensional case we can compare the numerical results only with the numerical result obtained by the finest stochastic discretization given by HSG-FV.

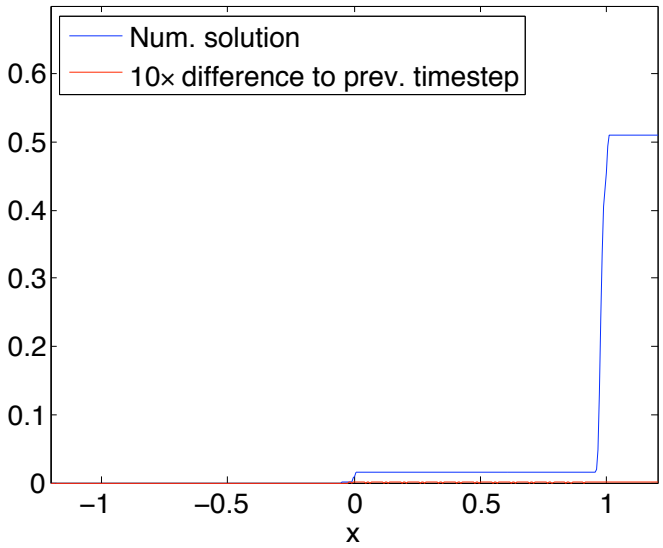

Fig. 1 Steady state $u_{\mathrm{F}} = 0.15$, $T = 10^6$ for the 1D model. Blue line: (deterministic) numerical solution, red line: difference to previous time step.

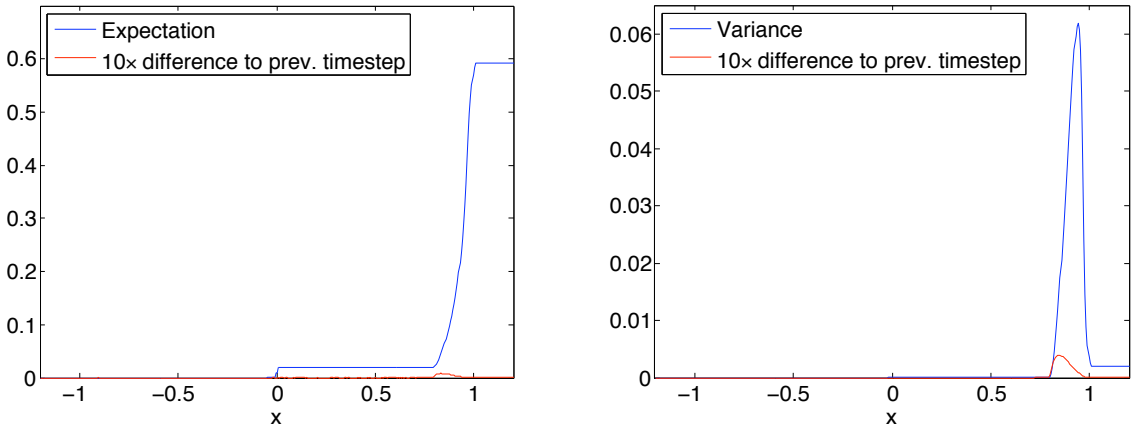

Fig. 2 Numerical solution for the 1D model at $T = 10^6$ and $u_{\mathrm{F}} = 0.15 + 0.05\theta$ computed with HSG-FV method for $N_{\mathrm{r}} = 4$, $N_{\mathrm{o}} = 4$. (a) Expectation (blue line) and the difference to the previous time-step (red line). (b) Variance (blue line) and the difference to the previous time-step (red line).

3.4.1 Numerical experiments in one space dimension

The point of interest of the application is to determine the steady state of solutions of (9) with respect to the uncertainty, represented by the random variable θ. In particular the random input is given by the random perturbed feed $u_F = 0.15 + c\theta$, with $c \in \mathbb{R}$ and a random variable θ uniformly distributed on the interval $[0, 1]$ ($\theta \sim \mathcal{U}(0, 1)$). Thus, the unknown u depends on the random variable θ and the solution may or may not attain a steady state depending on the value of θ. In Section 5.1 we discuss the appropriate conditions on γ^1, γ^2, u_{F} and b. For example a steady state can be achieved for the (deterministic) choice $u_{\mathrm{F}} \equiv 0.15$. Figure 1 shows the numerical solution for this case at the time $T = 10^6$. The plot of the difference to the previous time step (red line) shows that there is no difference to the previous timestep. In other words the solution shown is stationary.

We assume that the random variable θ is uniformly distributed on the interval $[0, 1]$ ($\theta \sim \mathcal{U}(0, 1)$). For this case we consider the problem (9) with $u_{\mathrm{F}} = 0.15 + 0.05\theta$. Figures 2 and Figure 3 show the most important stochastic quantities of the numerical solution. In particular Figure 2 shows the expectation and the variance of the numerical solution at $T = 10^6$, and Figure 3 shows the expectation and the sum of the expectation and the standard deviation for the same setting.

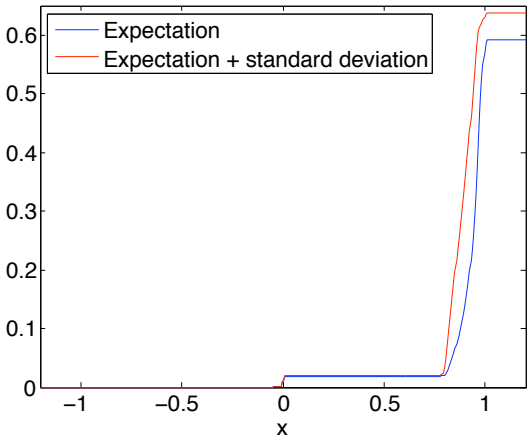

Fig. 3 Numerical solution for the 1D model at $T = 10^6$ and $u_{\mathrm{F}} = 0.15 + 0.05\theta$ computed with HSG-FV method for $N_{\mathrm{r}} = 4$, $N_{\mathrm{o}} = 4$. Expectation (blue line) and expectation + standard deviation (red line).

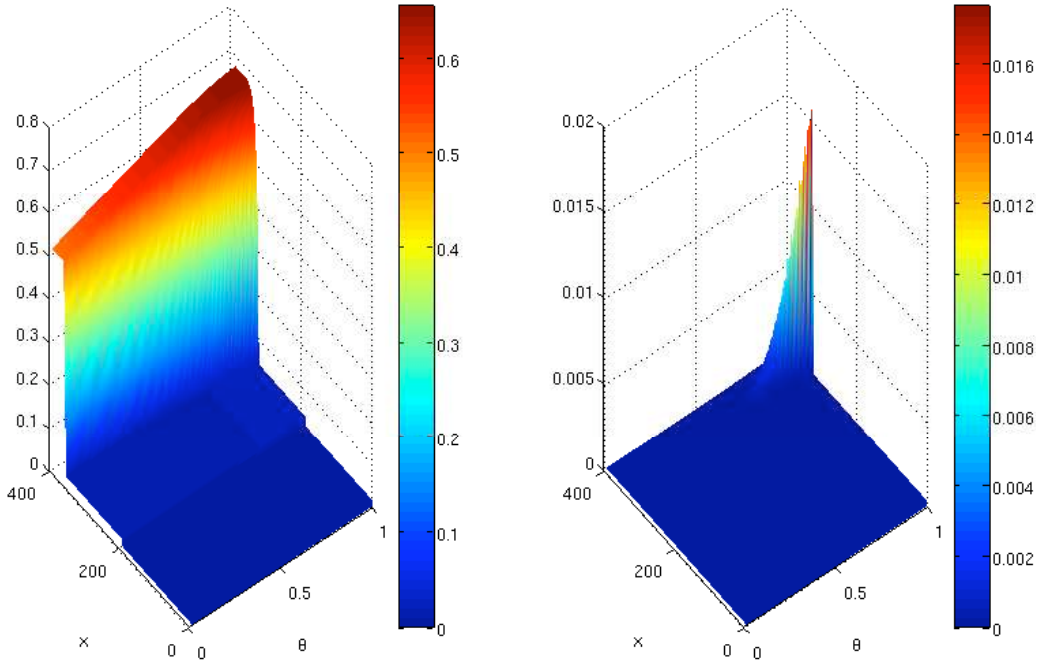

Fig. 4 Distribution of the HSG-FV numerical solution for the 1D model at $T = 10^6$ with $u_{\mathrm{F}} = 0.15 + 0.05\theta$ (left) and the difference to the previous time-step (right).

The HSG-FV representation of the numerical solution allows a memory-efficient storage of simulation data. We only save the coefficients $u^0, \ldots, u^P$ for each mesh point and timestep. But these data allow us to reconstruct the numerical solution for each value of $\theta \in [0, 1]$. Consequently, we can consider not only the expectation (Fig. 2(a)) and the variance (Fig. 2(b)) of the solution, but we also get, without sophisticated computation, the distribution of the numerical solution and the distribution of the difference to the previous timestep (see Fig. 4 with respect to $\theta \in [0, 1]$ (θ-axis)).

The further discussion of advantages of the method requires the comparison with Monte-Carlo and SG-FV methods. To make this comparison possible we make two changes in our setting: To make comparable simulations with the Monte-Carlo approach we reduce the time T to $T = 2.5 \cdot 10^5$. To stress the influence of the uncertainty we consider $u_{\mathrm{F}} = 0.15 + 0.5\theta$, with $\theta \sim \mathcal{U}(0, 1)$. For all one-dimensional computations in this paper we use an equidistant mesh with 400 points on

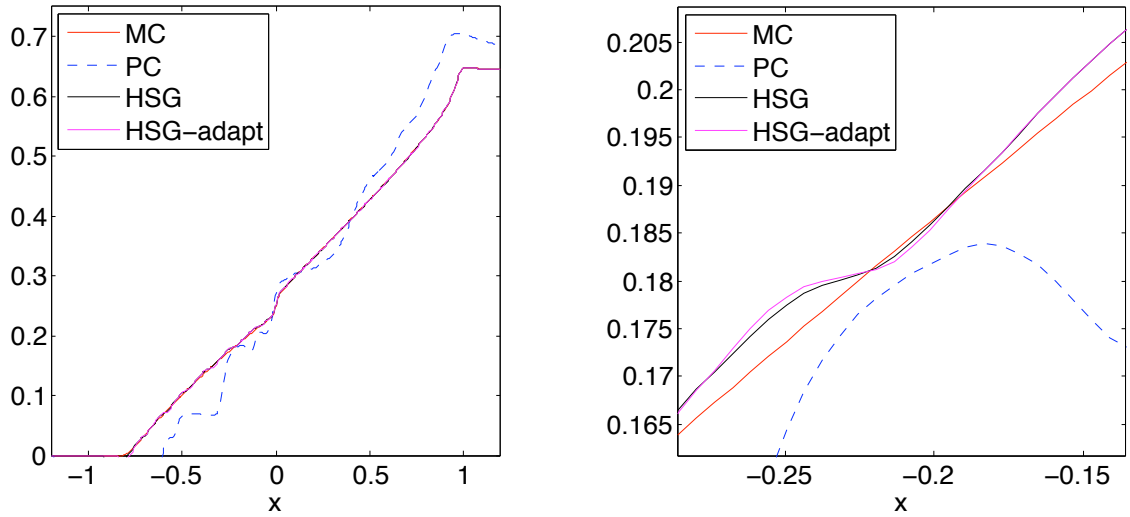

Fig. 5 Plot (a) shows the expectation for the 1D model, $T = 2.5 \cdot 10^5$ and $u_{\mathrm{F}} = 0.15 + 0.5\theta$ computed with different numerical methods MC-FV with 500000 samples, SG-FV $N_{\mathrm{o}} = 8$, HSG-FV with $N_{\mathrm{o}} = 4$, $N_{\mathrm{r}} = 4$ and HSG-adapt with $N_{\mathrm{o}} = 4$, $N_{\mathrm{r}} = 4$. Plot (b) is an enlarged view of a portion of plot (a).

Samples	50000	100000	200000	400000
L^1-error	5.61e-03	1.39e-03	1.13e-03	6.65e-04

Table 1 L^1-error for the MC-FV approach. Numerical experiment in one space dimension.

	HSG-FV without adaptivity			HSG-FV with adaptivity		
N_{o}	$N_{\mathrm{r}} = 3$	$N_{\mathrm{r}} = 4$	$N_{\mathrm{r}} = 5$	$N_{\mathrm{r}} = 3$	$N_{\mathrm{r}} = 4$	$N_{\mathrm{r}} = 5$
2	1.41e-02	4.25e-03	1.42e-03	1.41e-02	4.25e-03	1.42e-03
3	1.00e-02	3.13e-03	1.02e-03	1.05e-02	3.51e-03	1.08e-03
4	7.38e-03	2.32e-03	7.79e-04	8.36e-03	2.65e-03	8.47e-04
5	5.42e-03	1.64e-03	6.37e-04	6.15e-03	2.05e-03	7.78e-04

Table 2 L^1-error of the HSG-FV approach without adaptivity (Sect. 3.4.1) and with adaptivity (Sect. 4.4) with threshold parameter 0.01. Numerical experiment in one space dimension.

SG-FV without adaptivity				SG-FV with adaptivity			
N_{o}	L^1-error	N_{o}	L^1-error	N_{o}	L^1-error	N_{o}	L^1-error
6	1.20e-01	10	7.56e-02	6	1.15e-01	10	7.51e-02
7	1.02e-01	11	6.70e-02	7	9.74e-02	11	6.58e-02
8	9.52e-02	12	6.28e-02	8	8.92e-02	12	7.33e-02
9	8.16e-02			9	7.72e-02		

Table 3 L^1-error of the SG-FV approach without adaptivity (Sect. 3.4.1) and with adaptivity (Sect. 4.4) with threshold parameter 0.01.

the interval $[-1.2, 1.2]$. The reference solution is given by the Monte-Carlo numerical solution, computed with 500000 samples.

We begin our comparison with Figure 5(a), which provides an overview on the accuracy of the methods compared. Figure 5(a) shows expectations of the MC-FV, SG-FV, and HSG-FV approaches (with and without adaptivity) for this setting. Usually for small stochastic influence the SG-FV method provides an accurate solution for the polynomial order $N_{\mathrm{o}} = 8$. But already for $u_F = 0.15 + 0.5\theta$ this method is no longer sufficiently accurate. On the other hand, the plot of the HSG-FV solution matches the MC-FV result almost exactly, such that we need a zoom as in Figure 5(b) to show some difference between MC and HSG approaches.

N_o	Adaptivity	$N_r = 3$	$N_r = 4$	$N_r = 5$	N_o	Adaptivity	$N_r = 3$	$N_r = 4$	$N_r = 5$
2	without adaptivity	950	1590	3794	4	without adaptivity	3297	5630	13781
	N_o-adaptivity	961	1570	3746		N_o-adaptivity	3009	5070	12061
	N_r-adaptivity	716	1113	2383		N_r-adaptivity	2568	3931	8319
	$N_r + N_o$-adaptivity	678	1093	2325		$N_r + N_o$-adaptivity	2303	3566	7459
3	without adaptivity	1852	3172	7655	5	without adaptivity	5530	9581	22389
	N_o-adaptivity	1767	2916	6918		N_o-adaptivity	4977	8421	20310
	N_r-adaptivity	1436	2215	4638		N_r-adaptivity	4589	7512	17115
	$N_r + N_o$-adaptivity	1304	2002	4306		$N_r + N_o$-adaptivity	4098	6708	14923

Table 4 Duration (in seconds) of HSG-FV(-adapt) computation on Intel(R) Core(TM)2 Quad CPU Q9550 (2.83GHz)s with adaptivity with threshold parameter 0.001.

	Number of samples				
	50000	100000	200000	400000	500000
Time	24009	47651	96005	192019	353391

Table 5 Duration (in seconds) of MC-FV computations on 32 CPUs. Computed on AMD Opteron(tm) Processor 2376 (2.3GHz)

	$N_o = 6$	$N_o = 7$	$N_o = 8$	$N_o = 9$	$N_o = 10$	$N_o = 11$	$N_o = 12$
without N_o-adaptivity	703	1510	3146	6859	13038	27413	53822
with N_o-adaptivity	652	1422	2849	6396	12197	26107	50403

Table 6 Duration (in seconds) of SG-FV computations on 4 CPUs without and with polynomial order adaptivity. Time in sec.

	Computed on 4 CPUs				Computed on 16 CPUs	
N_o	$N_r = 2$	$N_r = 3$	$N_r = 4$	$N_r = 5$	$N_r = 4$	$N_r = 5$
2	350	1021	1674	3949		
3	721	2055	3362	7920		
4	1332	3767	6032	14427	1753	4188
5	2277	6069	10195	24346	2701	6351

Table 7 Duration (in seconds) of HSG-FV computations on Intel-Xeon E7-4830 (2.13GHz) without adaptivity.

To consider the L^1-error of the numerical solution we refer to Table 1, Table 2, and Table 3. Table 1 shows the L^1-error of the MC-FV method for several numbers of samples. Table 2 shows the L^1-error of the HSG-FV numerical solution with $N_o = 2, \ldots, 5$ and $N_r = 3, \ldots, 5$, Table 3 shows the L^1-error of the SG-FV numerical solution ($N_r = 0$) for $N_o = 6, \ldots, 12$. We can see, that the L^1-error of the HSG-FV method is comparable with the L^1-error of the MC method. But on the other hand Table 4, Table 5, Table 6, and Table 7 show that the computational effort of the HSG-FV method is significantly lower than the effort of the MC-FV method. To summarize, the computations with the HSG-FV method on a Quad Core desktop computer are 8.5 times faster, than the MC computations on 32 CPU's.

The further reduction of the computation time of the HSG-FV method by the parallelisation and adaptivity will be discussed in Section 3.5 and Section 4.

3.4.2 Numerical experiments in two space dimensions

We consider the HSG approach (18) with functions $\mathbf{q}$, b and u_F defined in Section 5.2 and in the Appendix. We use the 2D finite volume method introduced in Section 3.3.4. Figure 6(a) and Figure 6(b) show the expectation and variance of the numerical solution computed with HSG-FV method in two space dimensions at time $T = 10^5$. We performed this computation with $N_r = 2$ and $N_o = 2$ ($\dim S^{N_o, N_r} = 12$).

A comparable result with the MC-FV method in two space dimensions is not possible with nowadays computer power. Therefore we compare our numerical results with the most fine HSG-FV solution we could realize, that means $N_r = 3$ and $N_o = 3$. The Table 8 shows the L^1-error for $N_r = 1, \ldots, 3$ and $N_o = 1, \ldots 3$.

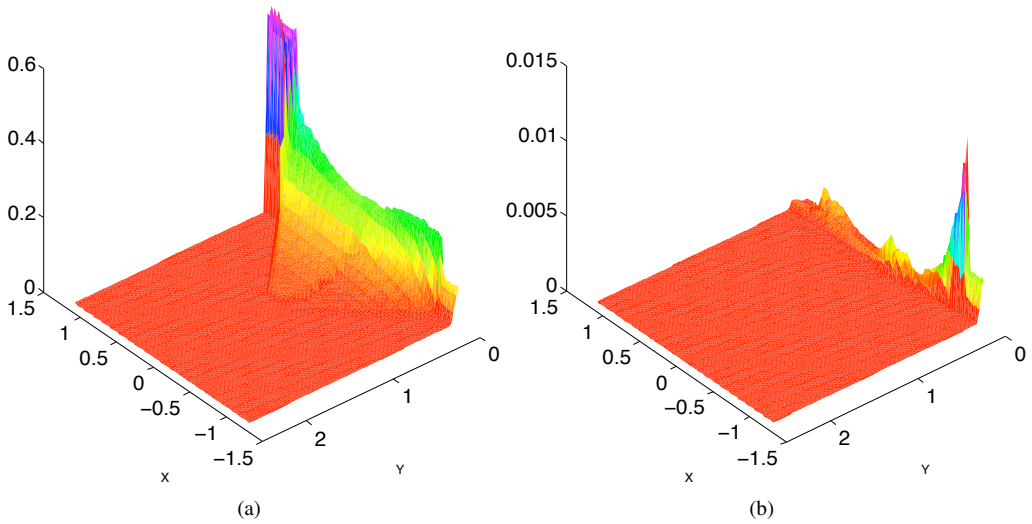

Fig. 6 Figure (a) Expectation (a) and Variance (b) for the 2D model of the HSG-FV approach with $N_\mathrm{r} = 2$, $N_\mathrm{o} = 2$, $u_F = 0.15 + 0.05\theta$ for $T = 10^5$.

	$N_\mathrm{r} = 1$	$N_\mathrm{r} = 2$	$N_\mathrm{r} = 3$
$N_\mathrm{o} = 1$	5.04e-03	2.98e-03	7.82e-04
$N_\mathrm{o} = 2$	4.13e-03	2.31e-03	3.49e-04
$N_\mathrm{o} = 3$	3.95e-03	2.29e-03	0

Table 8 L^1-error for $T = 2.5 \cdot 10^5$ and $u_F = 0.15 + 0.25\theta$ compared with the HSG-FV numerical solution with $N_\mathrm{r} = 3$, $N_\mathrm{o} = 3$.

3.5 The benefits of the parallel application

The application of the stochastic Galerkin approach yields a high dimensional system. The structure of this system allows the parallel computation of the coefficients $u^0, \ldots, u^P$ in each time-step. In the sections below we give a short overview over the SG-FV and HSG-FV approaches from a parallelisation point of view.

3.5.1 SG-FV approach

The SG-FV approach, typically with $N_\mathrm{r} = 0$ and $N_\mathrm{o} \geq 4$ allows the parallelisation according to the polynomial order. Because the system is not decoupled the values should be synchronised in each time step. This implies, that the efficient parallelisation requires fast communication. In particular this can be achieved by using shared memory machines and OpenMP. The computational effort can be further reduced by N_o-adaptivity, we refer to the Section 4.3 for details.

3.5.2 HSG-FV approach

The stochastic dimension of the system increases with N_r. However the system (18) is decoupled in the stochastic element index, which means that the coefficient $u_{p,l}^{N_\mathrm{r}}(\mathbf{x}_1, t_1)$ for $p = 0, \ldots, N_\mathrm{o}$, $l = 0, \ldots, 2^{N_\mathrm{r}} - 1$ and $(\mathbf{x}_1, t_1) \in D_T$ does not depend on $u_{q,k}^{N_\mathrm{r}}(\mathbf{x}_2, t_2)$ for each choice of $q = 0, \ldots, N_\mathrm{o}$, $k = 0, \ldots, 2^{N_\mathrm{r}} - 1$ and $(\mathbf{x}_2, t_2) \in D_T$ if $k \neq l$. The solution on each stochastic element $I_l^{N_\mathrm{r}}$, $l = 0, \ldots, 2^{N_\mathrm{r}} - 1$, can be computed without any synchronisation with the solutions on $I_k^{N_\mathrm{r}}$, $k \neq l$ during the computation. This allows efficient parallelisation on distributed memory machines, for example with MPI. In particularly the higher number of resolution allows using up to 2^{N_r} CPUs (or nodes) without synchronisation during the computation.

Table 7 shows the computation times on 4 and 16 CPUs for the numerical example in one space dimension. For the higher numbers of CPUs we refer to Table 9, which shows the decrease of computation time with increasing number of CPUs for $N_\mathrm{r} = 7$ and $N_\mathrm{o} = 3$ and $N_\mathrm{o} = 4$ computed on 4 to 128 CPUs and $N_\mathrm{r} = 8$ and $N_\mathrm{o} = 3$ on 4 to 128 CPUs for the numerical example in one space dimension. The computational effort can be reduced by N_o- and N_r-adaptivity, where the count of CPUs (or nodes) used determines the coarsest refinement level of N_r-adaptivity. We refer to Section 4 for details.

	Number of CPUs					
	4	8	16	32	64	128
$N_\mathrm{r} = 7$, $N_\mathrm{o} = 3$	42459	21377	10770	5471	2804	1525
$N_\mathrm{r} = 7$, $N_\mathrm{o} = 4$	77012	38696	19470	9824	5015	2673
$N_\mathrm{r} = 8$, $N_\mathrm{o} = 3$	102504	43422	21599	11361	5889	2973

Table 9 HSG-FV computation times for $N_\mathrm{r} = 7$, $N_\mathrm{o} = 3, 4$ and $N_\mathrm{r} = 8$, $N_\mathrm{o} = 3$.

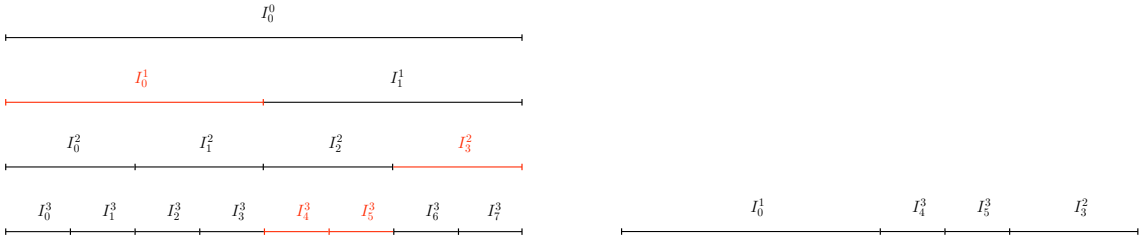

(a) Submeshes for $l = 0, \ldots, 3$ (b) Resulting mesh

Fig. 7 Sketch of the adapted graded tree structure for $L = 3$.

4 Adaptivity in the stochastic space

In this section we consider the possibilities to reduce the computational effort further by the adapting of the stochastic dimension. We consider two methods, namely N_r-adaptivity, which analyses and reduces the N_r-order, and N_o-adaptivity, which analyses and reduces so-called polynomial order. The concept of N_r-adaptivity requires a method for the computation of so called "details". This means the quantification of the information that will get lost by the re-coarsening step $N_\mathrm{r} \to N_\mathrm{r} - 1$. We use the concept of a multi-wavelet basis for this purpose. For further reading we refer to [9–11].

4.1 Multi-wavelet basis

Similarly to Section 3.3.1 we restrict our explanation to a unique stochastic dimension. Here $\theta = \theta(\omega)$ is again a random variable on the probability space (Ω, P) which satisfies $\theta \in L^2(\Omega)$ and $\theta \sim \mathcal{U}(0,1)$. For $N_\mathrm{o} \in \mathbb{N}_0$ and $N_\mathrm{r} \in \mathbb{N}_0$ let $S^{N_\mathrm{o},\,N_\mathrm{r}}$ be the space of piecewise-continuous polynomials as defined in (15). The orthogonal basis of $S^{N_\mathrm{o},\,N_\mathrm{r}}$ is given by rescaled Legendre polynomials $\phi^{N_\mathrm{r}}_{0,0}, \ldots, \phi^{N_\mathrm{r}}_{N_\mathrm{o},2^{N_\mathrm{r}}-1}$. The multi-wavelet subspace $W^{N_\mathrm{o},\,N_\mathrm{r}}$ is defined as the orthogonal complement of $S^{N_\mathrm{o},\,N_\mathrm{r}}$ in $S^{N_\mathrm{o},\,N_\mathrm{r}+1}$. The construction of the orthonormal wavelet basis is described in [2, 3, 28]. Let $\psi_0, \ldots, \psi_{N_\mathrm{o}}$ be an orthonormal basis of $W^{N_\mathrm{o},\,0}s$ that satisfies

$$\langle \psi_i,\, \psi_j \rangle = \delta_{ij}, \quad 0 \le i, j \le N_\mathrm{o}.$$

The relation $S^{N_\mathrm{o},\,0} \perp W^{N_\mathrm{o},\,0}$ implies

$$\langle \psi_j,\, x^i \rangle = 0, \qquad 0 \le i, j \le N_\mathrm{o}.$$

The space $W^{N_\mathrm{o},\,N_\mathrm{r}}$ is spanned by multi-wavelets $\psi^{N_\mathrm{r}}_{i,l}$ given by

$$\psi^{N_\mathrm{r}}_{i,l}(\xi) = 2^{N_\mathrm{r}/2}\psi_i(2^{N_\mathrm{r}}\xi - l), \quad i = 0, \ldots, N_\mathrm{o}, \quad l = 0, \ldots, 2^{N_\mathrm{r}} - 1,$$

and their support is $\mathrm{Supp}(\psi^{N_\mathrm{r}}_{i,l}) = I^{N_\mathrm{r}}_l := [2^{-N_\mathrm{r}}l, 2^{-N_\mathrm{r}}(l+1)]$.

4.2 N_r -adaptivity

The algorithm of the adaptive multiresolution scheme for two-dimensional problems was introduced in [9–11]. We use a concept of a two-dimensional graded tree for dealing with the HSG-FV data structure. As usual, a *node* is an element of the tree that represents a control volume of a local mesh, defined by the stochastic element I^l_j for $0 \le l \le L$ in (15). Here L denotes the level with the finest mesh. The *root* is the basis of the tree, represented by I^0_0. Each parent node has two children, and satisfies $I^l_i = I^{l+1}_{2i} \cup I^{l+1}_{2i+1}$. A node is called *leaf* when it has no children.

The goal of the N_r-adaptivity is to avoid unnecessary refinements and to reduce the number of nodes on which we perform the finite volume computation. For example, consider Figure 7. Figure 7(a) shows the structure of the graded tree for $L = 3$. The red marked nodes are included in the resulting mesh (Figure 7(b)).

Algorithm 1 Re-meshing

for $I_i^l \in N(\mathcal{L}(\Lambda))$ **do**
  if $I_{2i}^{l+1} \in \mathcal{L}(\Lambda)$ **and** $d_{(2i),(i)}^{l+1} > \varepsilon$ **then**
    $\Lambda^{\mathrm{ref}} \leftarrow \Lambda^{\mathrm{ref}} \cup (2i)$
  end if
  if $I_{2i+1}^{l+1} \in \mathcal{L}(\Lambda)$ **and** $d_{2i+1,i}^{l+1} > \varepsilon$ **then**
    $\Lambda^{\mathrm{ref}} \leftarrow \Lambda^{\mathrm{ref}} \cup (2i+1)$
  end if
  if $I_{2i}^{l+1} \in \mathcal{L}(\Lambda)$ **and** $I_{2i+1}^{l+1} \in \mathcal{L}(\Lambda)$ **then**
    if $d_{2i,i}^{l+1} < \varepsilon$ **and** $d_{2i+1,i}^{l+1} < \varepsilon$ **then**
      $\Lambda^{\mathrm{del}} \leftarrow \Lambda^{\mathrm{del}} \cup (2i) \cup (2i+1)$
    end if
  end if
end for
for $(i,l) \in \Lambda^{\mathrm{del}}$ **do**
  if $l > C$ **then**
    $\Lambda \leftarrow \Lambda \setminus (i,l)$
  end if
end for
for $(i,l) \in \Lambda^{\mathrm{ref}}$ **do**
  $\Lambda \leftarrow \Lambda \cup (2i, l+1) \cup (2i+1, l+1)$
end for

Algorithm 2 Finite volume method with N_{r}-adaptivity

while $t < T$ **do**
  Calculate $\triangle t$.
  Compute $u(t + \triangle t)$ for all leaves in $\mathcal{L}(\Lambda)$.
  Re-mesh (Algorithm 1).
  $t \leftarrow t + \triangle t$
end while

We start with the description of the re-meshing subroutine. We recall, that Λ denotes the set of the indices of the existing nodes, $\mathcal{L}(\Lambda)$ denotes the set of leaves and $N(\mathcal{L}(\Lambda))$ is the set of parents of the elements in $\mathcal{L}(\Lambda)$. The sets Λ^{del} and Λ^{ref} contain the indices of nodes that should be deleted respectively refined. Our idea is to consider the difference of the data on the active leaves and the projection on their parent node. We decided to use the multi-wavelet basis introduced in Section 4.1 for this purpose. In particular, this means for the random field $w \equiv w(x,t,\theta(\omega)) \in L^2(\Omega)$ that a leaf I_i^{l+1} with a parent node I_j^l, the "detail" coefficient $d_{i,j}^{l+1}$ is given by

$$d_{i,j}^{l+1} := \sum_{n=0}^{N_{\mathrm{o}}} \left| \left\langle \sum_{p=0}^{N_{\mathrm{o}}} w_{p,i}^{l+1} \phi_{p,i}^{l+1},\ \psi_{n,j}^{n,l} \right\rangle \right|.$$

We define the tolerance ε and the coarsest refinement level $C \geq 0$. In our computations C is given by the number of CPUs used. For example, Figure 8 shows the distribution of the refinement levels with $C = 1$ at $T = 10^6$. Algorithm 1 explains our re-meshing procedure. Together with the re-meshing algorithm we can introduce an algorithm for the computation of the numerical solution (Algorithm 2). For the computation of the numerical flux between elements with the different refinement level we use virtual nodes with the finer refinement level.

4.3 Polynomial order adaptivity

Theother kind of adaptivity, that we introduce is a polynomial-order adaptivity or N_{o}-adaptivity. Let $w = w(\mathbf{x},t,\theta(\omega))$ be again a random field with finite variance. The main idea is to omit those polynomial coefficients that satisfy $|w_{p,i}^l| < \varepsilon_l$ for $l = 0,\ldots,N_{\mathrm{r}}$, $p = 0,\ldots,N_{\mathrm{o}}$ and $i = 0,\ldots,2^{2l}-1$. For a given threshold parameter ε we define $\varepsilon_l = \varepsilon \cdot 2^{-l/2}$. For sake

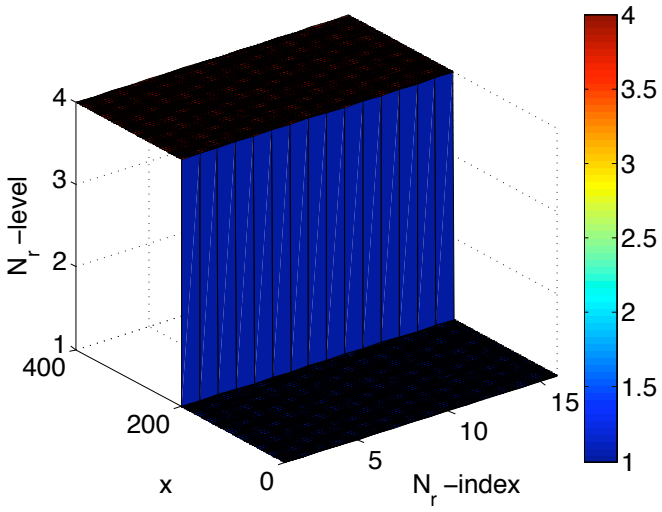

Fig. 8 Distribution of the used N_r levels at $T = 10^6$ with $u_\mathrm{F} = 0.15 + 0.05\theta$ computed with the finest N_r-level 4 and the coarsest level 1.

Algorithm 3 N_o–adaptivity

for $I_n^l \in \mathcal{L}(\Lambda)$ **do**
  $p \leftarrow M\,(n)$.
  if $\left|w_{p,n}^l\right| < \varepsilon_l$ **then**
    delete $\{w_n^p\}$.
    $M\,(n) \leftarrow p - 1$
  else
    add $\left\{w_n^{p+1}\right\}$.
    $M\,(n) \leftarrow p + 1$
  end if
end for

Algorithm 4 Finite volume method with N_o and N_r-adaptivity

while $t < T$ **do**
  Calculate $\triangle t$.
  Compute $u(t + \triangle t)$ for all leaves in $\mathcal{L}(\Lambda)$.
  Re-mesh (Algorithm 1).
  Adapt Polynomial Order (Algorithm 3).
  $t \leftarrow t + \triangle t$
end while

of brevity we consider $l = N_\mathrm{r}$. We extend the definition of the projection $\Pi^{N_\mathrm{r},N_\mathrm{o}}\,[w]$ to

$$\Pi_{P-ad}^{N_\mathrm{r},N_\mathrm{o}}\,[w]\,(\mathbf{x},t,\theta(\omega)) := \sum_{i=0}^{2^{N_\mathrm{r}}-1}\sum_{p=0}^{M\,(i)} w_{p,i}^{N_\mathrm{r}}(\mathbf{x},t)\phi_{p,i}^{N_\mathrm{r}}\big(\theta(\omega)\big).$$

Here $M\,(i) \leq N_\mathrm{o}$ is the highest polynomial order used on the stochastic element I_i^l. Algorithm 3 describes the N_o-adaptivity method. Together with the Algorithm 2 (resp. Algorithm 1) we obtain the N_r- and N_o- **adaptive finite volume method** (HSG-FV-adapt) described in Algorithm 4.

4.4 Summary

In direct comparison (with appropriate settings) the N_r-adaptivity is more efficient and accurate as N_o-adaptivity. On the other hand N_r–adaptivity method requires expensive computations and requires higher programming effort. Both methods can be used together with parallel computing. The Figure 5(a) shows the comparison of numerical solutions of the

	HSG-FV, N_r-adaptivity, no polynomial adaptivity			HSG-FV, N_r-adaptivity with polynomial adaptivity		
N_o	$N_\mathrm{r}=3$	$N_\mathrm{r}=4$	$N_\mathrm{r}=5$	$N_\mathrm{r}=3$	$N_\mathrm{r}=4$	$N_\mathrm{r}=5$
2	1.41e-02	4.33e-03	1.83e-03	1.45e-02	5.30e-03	3.52e-03
3	1.01e-02	3.20e-03	1.13e-03	1.14e-02	4.31e-03	3.37e-03
4	7.41e-03	2.46e-03	9.36e-04	8.40e-03	2.86e-03	1.72e-03
5	5.42e-03	1.64e-03	6.37e-04	6.15e-03	2.05e-03	7.78e-04

Table 10 L^1-error of the HSG-FV approach with N_r-adaptivity with threshold parameter 0.001 without polynomial adaptivity, and with polynomial order adaptivity with threshold parameter 0.01.

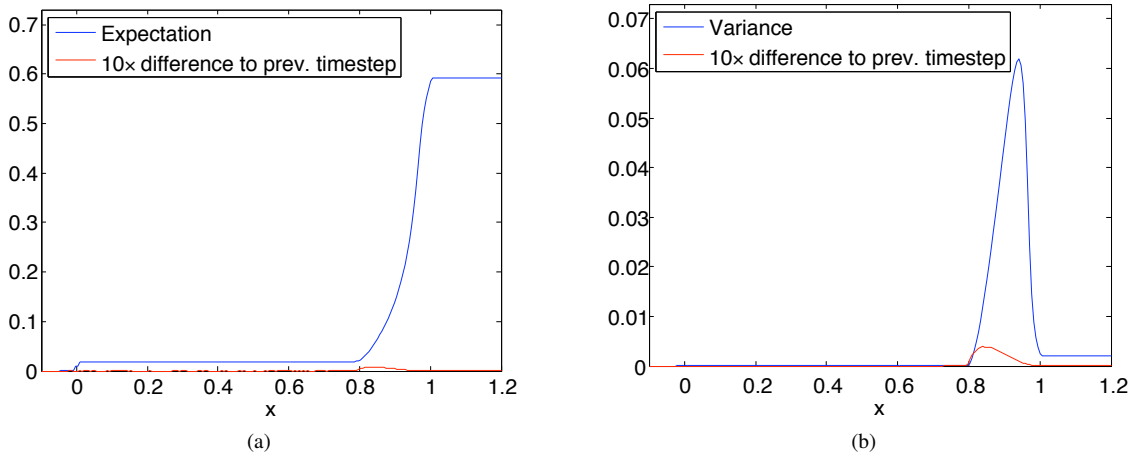

Fig. 9 HSG-FV-adapt numerical solution for the 1D model at $T=10^6$ with $u_\mathrm{F}=0.15+0.05\theta$ computed with $N_\mathrm{r}=4$, $N_\mathrm{o}=4$, N_r–adaptivity parameter 0.001 and N_o–adaptivity parameter 0.01. (a) Expectation (blue line) and the difference to the previous time-step. (b) Variance.

equation (9) computed with and without adaptivity together with the MC-FV solution. The Figure 9 and Figure 10 show expectation, variance and the distribution of the adaptive numerical solution. We refer to Tables 2 and 10 for the L^1-error of the HSG finite volume approach with and without adaptivity. Table 3 contains the L^1-error of the SG-approach with and without adaptivity. The computation times on a Quad-Core CPU for HSG and SG methods with and without adaptivity are shown in Table 4 and Table 6 respectively.

5 Details of the flux construction

5.1 One-dimensional clarifier-thickener model

Let us define the function

$$\tilde{b}(u)=\begin{cases} u_\infty u(1-u)^{n_\mathrm{RZ}} & \text{for } 0\le u\le 1,\\ 0 & \text{for } u<0 \text{ and } u>1.\end{cases} \tag{20}$$

Then the function b is given by the following expression;

$$b(u)=\begin{cases} u_\infty u(1-u)^{n_\mathrm{RZ}} & \text{for } 0\le u\le u_*,\\ p_2(u) & \text{for } u_*<u\le u_\mathrm{max}:=u_*-\tilde{b}(u_*)/\tilde{b}'(u_*),\\ 0 & \text{for } u>u_\mathrm{max}.\end{cases} \tag{21}$$

Here $p_2(u)=\alpha u^2+\beta u+\gamma$ is the unique second-order polynomial satisfying $p_2(u_*)=\tilde{b}(u_*)$, $p_2'(u_*)=\tilde{b}'(u_*)$ and $p_2(u_\mathrm{max})=0$. The insertion of p_2 between u_* and u_max ensures that the function b is Lipschitz continuous with support on $[0,u_\mathrm{max}]$, and continuously differentiable on $(0,u_\mathrm{max})$, and at the same time the left-sided derivative at u_max is negative.

Here, u_∞ is the so-called Stokes velocity, that is, the settling velocity of a single particle in an unbounded fluid. If we measure distance in meters and time in seconds, then a realistic value is $u_\infty=10^{-4}\,\mathrm{m/s}$, while a value for the exponent

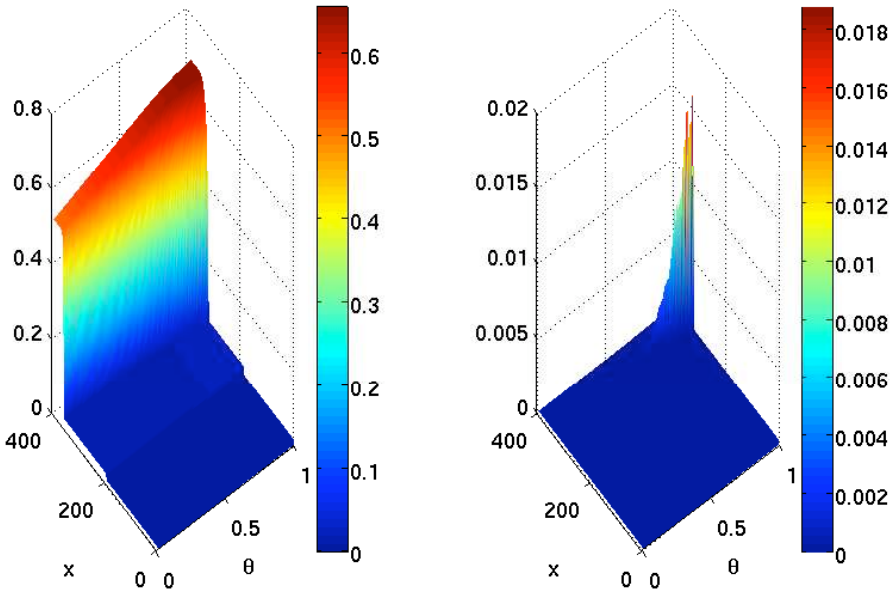

Fig. 10 Distribution of the HSG-FV-adapt numerical solution for the 1D model at $T = 10^6$ with $u_{\mathrm{F}} = 0.15 + 0.05\theta$ and the difference to the previous time-step computed with N_{r}-adaptivity parameter 0.001 and N_{o}-adaptivity parameter 0.01.

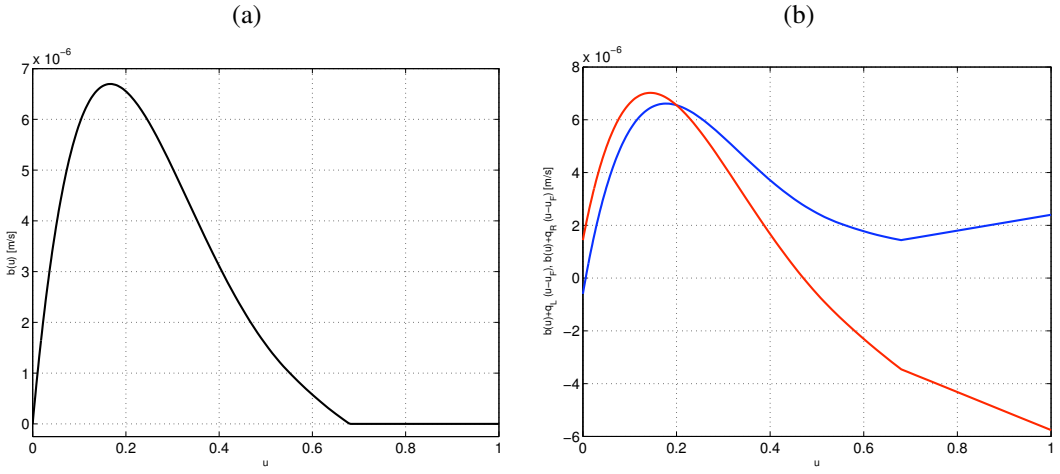

Fig. 11 (a) Batch flux density function $b(u)$ given by (20), (21) with $u_\infty = 10^{-4}\,\mathrm{m/s}$, $n_{\mathrm{RZ}} = 5$ and $u_* = 0.6$, (b) Fluxes $b(u) + q_{\mathrm{R}}(u - u_{\mathrm{F}})$ in the thickening zone (blue) and $b(u) + q_{\mathrm{L}}(u - u_{\mathrm{F}})$ in the sedimentation zone (red).

in (21) is $n_{\mathrm{RZ}} = 5$. If we choose, moreover, $u_* = 0.55$ and $u_{\max} = 0.657608695652174$ which is a realistic maximum packing density. Figure 11 (a) shows the function $b(u)$.

We now wish to operate the unit at a steady state, and consider later perturbations of the feed parameters that give rise to this steady state. To this end consider a cylindrical clarifier-thickener, i.e., we assume that the cross-sectional area A is constant. We assume that the bulk flows $Q_{\mathrm{L}} \le 0$, and $Q_{\mathrm{R}} \ge 0$ are given, and define $Q_{\mathrm{F}} := Q_{\mathrm{R}} - Q_{\mathrm{L}}$ and $q_{\mathrm{F}} := Q_{\mathrm{F}}/A$, $q_{\mathrm{L}} := Q_{\mathrm{L}}/A$ and $q_{\mathrm{R}} := Q_{\mathrm{R}}/A$.

As an example, let us consider the parameters $u_{\mathrm{F}} = 0.15$, $q_{\mathrm{L}} = -7.2 \times 10^{-6}\,\mathrm{m/s}$ and $q_{\mathrm{R}} = 3.0 \times 10^{-6}\,\mathrm{m/s}$. Then there is a steady state in the thickening zone with a jump between $u_{\mathrm{M}} = 0.68$ and $u_{\mathrm{m}} = 0.006704479177$, where u_{m} is the smallest solution of the equation $(q_{\mathrm{R}} - q_{\mathrm{L}})u_{\mathrm{F}} = q_{\mathrm{R}}(u - u_{\mathrm{F}}) + b(u)$. To be definite, we assume that the unit occupies the

depth interval $x \in [-1, 1]$ (in meters), where $x = x_{\mathrm{L}} = -1$, $x = 0$ and $x = x_{\mathrm{R}} = 1$ are the overflow, feed, and discharge levels, respectively. The control parameters correspond to a stationary discontinuity between u_{m} and u_{M}.

5.2 Two-dimensional models

Let us again consider the problem (11). We consider the flow field $\mathbf{q} : D_T \to \mathbb{R}^2$ defined by

$$\mathbf{q}(x, y) := \begin{cases} \mathbf{q}_L(x, y) & \text{for } x < 0 \\ \mathbf{q}_R(x, y) & \text{for } x > 0. \end{cases}$$

We construct $\mathbf{q}_L$ and $\mathbf{q}_R$ according to the Section A with $q_l(y) = 1.6 \cdot 10^{-6} y^2 - 7.2 \cdot 10^{-6}$ and $q_r(y) = -1.6 \cdot 10^{-6} y^2 + 3 \cdot 10^{-6}$ respectively. The boundary $\bar{y}$ is given by

$$\bar{y}(x) := \begin{cases} 0.2 & \text{for } x < -1 \\ x + 1.2 & \text{for } -1 \le x < -0.2 \\ 1 & \text{for } -0.2 \le x < 0.2 \\ -1 \cdot x + 1.2 & \text{for } 0.2 \le x < 1 \\ 0.2 & \text{for } 1 \le x. \end{cases}$$

The Figure 12 shows the resulting flow field $\mathbf{q} = (q^x, q^y)$. For our computations we use again the function b defined in (21) and $u_{\mathrm{F}} = 0.15 + 0.05\theta$ for $\theta \sim \mathcal{U}(0, 1)$.

A Appendix: construction of a divergence-free flow field

Let us consider the domain

$$\Omega := \big\{(x, y) \in \mathbb{R}^2 : \, x \ge 0, \; 0 \le y \le \bar{y}(x)\big\},$$

where we assume that $\bar{y}$ is a smooth curve, $\bar{y}(x) \ge y_{\min}$ for all $x \ge 0$ and we define $\bar{y}_0 := \bar{y}(0)$. The domain Ω is one half of a domain that represents either the cross-sectional area of an infinite cylindrical channel, where $x = 0$ is the plane of symmetry, or Ω is one half of the cross section of an axisymmetric domain, where $x = 0$ is the axis of symmetry. The first and second case correspond to the parameter values $\sigma = 0$ and $\sigma = 1$, respectively. We wish to determine solutions $\mathbf{q} = (q^x, q^y)$ to

$$\nabla \cdot \mathbf{q} \equiv \partial_x q^x + y^{-\sigma} \partial_y (y^\sigma q^y) = 0 \tag{22}$$

subject to the boundary conditions

$$q^x(0, y) = q_{\mathrm{R}}(y) \quad \text{for } 0 \le y \le \bar{y}_0, \qquad q^y(0, y) = 0 \quad \text{for } 0 \le y \le \bar{y}_0, \qquad q^y(x, 0) = 0 \quad \text{for } x \ge 0,$$

and the following zero-flux boundary condition, where $\mathbf{n} = (\bar{y}'(x), -1)^{\mathrm{T}}$ is the normal vector from the outer boundary of Ω pointing into the domain:

$$q^x\big(x, \bar{y}(x)\big)\bar{y}'(x) - q^y\big(x, \bar{y}(x)\big) = 0, \quad x \ge 0. \tag{23}$$

Let us assume now that q^x is given by a similarity solution of the type

$$q^x(x, y) = p(x) q_{\mathrm{R}}\left(\frac{y}{\bar{y}(x)}\bar{y}_0\right), \tag{24}$$

where the factor $p(x)$ still needs to be determined. This means that

$$\partial_x q^x(x, y) = p'(x) q_{\mathrm{R}}\left(\frac{y}{\bar{y}(x)}\bar{y}_0\right) - p(x) q_{\mathrm{R}}'\left(\frac{y}{\bar{y}(x)}\bar{y}_0\right)\frac{y}{(\bar{y}(x))^2} y_0 \bar{y}'(x).$$

Now note that integrating (22) with respect to y, we get

$$q^y(x, y) = -y^{-\sigma}\int_0^y \eta^\sigma \partial_x q^x(x, \eta)\,\mathrm{d}\eta = y^{-\sigma}\left(\frac{p(x) y_0 \bar{y}'(x)}{(\bar{y}(x))^2} A(x, y) - p'(x) B(x, y)\right), \tag{25}$$

where we define the integrals

$$A(x,y) := \int_0^y q_{\mathrm{R}}'\left(\frac{\eta}{\bar{y}(x)}\bar{y}_0\right)\eta^{1+\sigma}\,\mathrm{d}\eta, \quad B(x,y) := \int_0^y q_{\mathrm{R}}\left(\frac{\eta}{\bar{y}(x)}\bar{y}_0\right)\eta^{\sigma}\,\mathrm{d}\eta.$$

Substituting $s = \eta\bar{y}_0/\bar{y}(x)$ we obtain

$$A\big(x,\bar{y}(x)\big) = \left(\frac{\bar{y}(x)}{\bar{y}_0}\right)^{1+\sigma}\alpha, \quad \alpha := \int_0^{\bar{y}_0} q_{\mathrm{R}}'(s)s^{1+\sigma}\,\mathrm{d}s, \tag{26}$$

$$B\big(x,\bar{y}(x)\big) = \left(\frac{\bar{y}(x)}{\bar{y}_0}\right)^{\sigma}\beta, \quad \beta := \int_0^{\bar{y}_0} q_{\mathrm{R}}(s)s^{\sigma}\,\mathrm{d}s. \tag{27}$$

Inserting (26) and (27) into (25) we get

$$q^y\big(x,\bar{y}(x)\big) = \frac{p(x)\bar{y}'(x)\alpha}{\bar{y}(x)\bar{y}_0^{\sigma}} - \frac{p'(x)\beta}{\bar{y}_0^{\sigma}}.$$

Combining this with (24) we get from (23) we obtain

$$p(x)q_{\mathrm{R}}(\bar{y}_0)\bar{y}'(x) - \frac{p(x)\bar{y}'(x)\alpha}{\bar{y}(x)\bar{y}_0^{\sigma}} + \frac{p'(x)\beta}{\bar{y}_0^{\sigma}} = 0,$$

which can be rearranged to give the following ODE for $p(x)$:

$$p'(x) + p(x)\frac{\bar{y}'(x)}{\beta}\left(q_{\mathrm{R}}(\bar{y}_0)\bar{y}_0^{\sigma} - \frac{\alpha}{\bar{y}(x)}\right) = 0,$$

which has the solution

$$p(x) = \left(\frac{\bar{y}(x)}{\bar{y}_0}\right)^{\alpha/\beta}\exp\left(-\frac{q_{\mathrm{R}}(\bar{y}_0)\bar{y}_0^{\sigma}}{\beta}\big(\bar{y}(x)-\bar{y}_0\big)\right).$$

Thus, the x-component of the sought function $\mathbf{q}(x,y)$ is given by

$$q^x(x,y) = \left(\frac{\bar{y}(x)}{\bar{y}_0}\right)^{\alpha/\beta}\exp\left(-\frac{q_{\mathrm{R}}(\bar{y}_0)\bar{y}_0^{\sigma}}{\beta}\big(\bar{y}(x)-\bar{y}_0\big)\right)q_{\mathrm{R}}\left(\frac{y}{\bar{y}(x)}\bar{y}_0\right).$$

Now, noting that

$$\begin{aligned} p'(x) &= \left(\frac{\bar{y}(x)}{\bar{y}_0}\right)^{\alpha/\beta}\exp\left(-\frac{q_{\mathrm{R}}(\bar{y}_0)\bar{y}_0^{\sigma}}{\beta}\big(\bar{y}(x)-\bar{y}_0\big)\right)\frac{\bar{y}'(x)}{\beta}\left[\frac{\alpha}{\bar{y}(x)} - q_{\mathrm{R}}(\bar{y}_0)\bar{y}_0^{\sigma}\right] \\ &= \frac{p(x)\bar{y}'(x)}{\beta}\left[\frac{\alpha}{\bar{y}(x)} - q_{\mathrm{R}}(\bar{y}_0)\bar{y}_0^{\sigma}\right], \end{aligned}$$

we get from (25)

$$q^y(x,y) = y^{-\sigma}p(x)\bar{y}'(x)\left[\frac{y_0}{(\bar{y}(x))^2}A(x,y) + \frac{1}{\beta}\left(q_{\mathrm{R}}(\bar{y}_0)\bar{y}_0^{\sigma} - \frac{\alpha}{\bar{y}(x)}\right)B(x,y)\right].$$

Acknowledgements R. B. acknowledges support by Fondecyt project 1090456 and CONICYT project Anillo ACT1118 (ANANUM). R. B. and I. K. also acknowledge support by BASAL project CMM, Universidad de Chile and Centro de Investigación en Ingeniería Matemática (CI^{2}MA), Universidad de Concepción. I. K. and C. R. would like to thank the German Research Foundation (DFG) for financial support of the project within the Cluster of Excellence in Simulation Technology (EXC 310/1) at the University of Stuttgart. We thank Stefan Diehl for comments that resulted in a number of improvements of this paper.

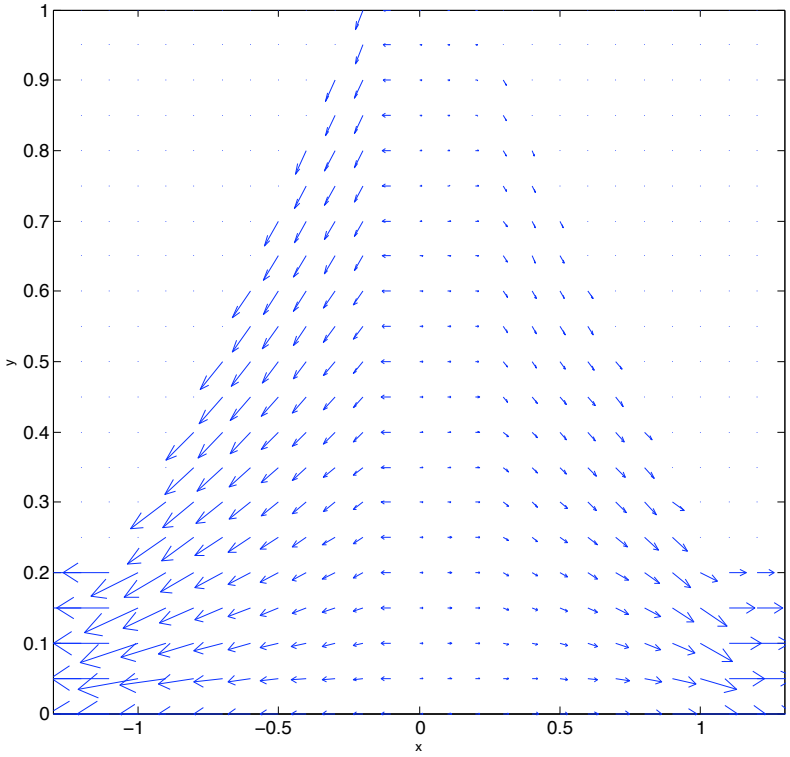

Fig. 12 "quiver"-plot of the vectorfield (q^x, q^y).

References

[1] R. Abgrall. A simple, flexible and generic deterministic apporach to uncertainty quantifications in non linear problems: application to fluid flow problems. 2007.

[2] B. K. Alpert. Wavelets and other bases for fast numerical linear algebra. In *Wavelets*, volume 2 of *Wavelet Anal. Appl.*, pages 181–216. Academic Press, Boston, MA, 1992.

[3] B. K. Alpert. A class of bases in L^2 for the sparse representation of integral operators. *SIAM J. Math. Anal.*, 24(1):246–262, 1993.

[4] E. Anderson, Z. Bai, C. Bischof, S. Blackford, J. Demmel, J. Dongarra, J. Du Croz, A. Greenbaum, S. Hammarling, A. McKenney, and D. Sorensen. *LAPACK Users' Guide*. Society for Industrial and Applied Mathematics, Philadelphia, PA, third edition, 1999.

[5] R. Bürger, K. H. Karlsen, N. H. Risebro, and J. D. Towers. Well-posedness in BV_t and convergence of a difference scheme for continuous sedimentation in ideal clarifier-thickener units. *Numer. Math.*, 97(1):25–65, 2004.

[6] R. Bürger, K. H. Karlsen, H. Torres, and J. D. Towers. Second-order schemes for conservation laws with discontinuous flux modelling clarifier-thickener units. *Numer. Math.*, 116:579–617, 2010.

[7] R. Bürger, K. H. Karlsen, and J. D. Towers. A model of continuous sedimentation of flocculated suspensions in clarifier-thickener units. *SIAM J. Appl. Math.*, 65(3):882–940, 2005.

[8] R. Bürger, K. H. Karlsen, and J. D. Towers. An Engquist-Osher-type scheme for conservation laws with discontinuous flux adapted to flux connections. *SIAM J. Numer. Anal.*, 47:1684–1712, 2009.

[9] R. Bürger, R. Ruiz, K. Schneider, and M. Sepúlveda. Fully adaptive multiresolution schemes for strongly degenerate parabolic equations in one space dimension. *M2AN Math. Model. Numer. Anal.*, 42(4):535–563, 2008.

[10] R. Bürger, R. Ruiz-Baier, and K. Schneider. Adaptive multiresolution methods for the simulation of waves in excitable media. *J. Sci. Comput.*, 43(2):261–290, 2010.

[11] R. Bürger, R. Ruiz-Baier, K. Schneider, and H. Torres. A multiresolution method for the simulation of sedimentation in inclined channels. *Int. J. Numer. Anal. Model.*, 9:479–504, 2012.

[12] R. Bürger, R. Ruiz-Baier, and H. Torres. A stabilized finite volume element formulation for sedimentation-consolidation processes. *SIAM J. Sci. Comput.*, 34:B265–B289, 2012.

[13] R. Bürger, W. L. Wendland, and F. Concha. Model equations for gravitational sedimentation-consolidation processes. *ZAMM Z. Angew. Math. Mech.*, 80(2):79–92, 2000.

[14] R. H. Cameron and W. T. Martin. The orthogonal development of non-linear functionals in series of Fourier-Hermite functionals. *Ann. of Math. (2)*, 48:385–392, 1947.

[15] J.-P. Chancelier, M. Cohen de Lara, and F. Pacard. Analysis of a conservation PDE with discontinuous flux: a model of settler. *SIAM J. Appl. Math.*, 54:954–995, 1994.

[16] S. Diehl. A conservation law with point source and discontinuous flux function modelling continuous sedimentation. *SIAM J. Appl. Math.*, 56(2):388–419, 1996.

[17] S. Diehl. Scalar conservation laws with discontinuous flux function: I. The viscous profile condition. *Comm. Math. Phys.*, 176:23–44, 1996.

[18] S. Diehl. Operating charts for continuous sedimentation. I. Control of steady states. *J. Engrg. Math.*, 41(2-3):117–144, 2001. Sedimentation and suspension flows: some recent contributions (Stuttgart, 1999).

[19] S. Diehl. Operating charts for continuous sedimentation. II. Step responses. *J. Engrg. Math.*, 53(2):139–185, 2005.

[20] S. Diehl. Operating charts for continuous sedimentation. III. Control of step inputs. *J. Engrg. Math.*, 54(3):225–259, 2006.

[21] S. Diehl. Operating charts for continuous sedimentation. IV. Limitations for control of dynamic behaviour. *J. Engrg. Math.*, 60(3-4):249–264, 2008.

[22] B. Engquist and S. Osher. One-sided difference approximations for nonlinear conservation laws. *Math. Comp.*, 36:321–351, 1981.

[23] R. G. Ghanem and P. D. Spanos. *Stochastic finite elements: a spectral approach*. Springer-Verlag, New York, 1991.

[24] James R. Kamm, William J. Rider, V. Gregory Weirs, Stefano Tarantola, and Marco Ratto. Sensitivity and uncertainty quantification techniques applied to systems of conservation laws. *Procedia - Social and Behavioral Sciences*, 2(6):7686 – 7687, 2010. ¡ce:title¿Sixth International Conference on Sensitivity Analysis of Model Output¡/ce:title¿.

[25] S. N. Kružkov. First order quasilinear equations with several independent variables. *Mat. Sb. (N.S.)*, 81 (123):228–255, 1970.

[26] Alexander Kurganov and Guergana Petrova. Central-upwind schemes on triangular grids for hyperbolic systems of conservation laws. *Numerical Methods for Partial Differential Equations*, 21(3):536–552, 2005.

[27] G. J. Kynch. A theory of sedimentation. *Trans. Faraday Soc.*, 48:166–176, 1952.

[28] O. P. Le Maître, H. N. Najm, R. G. Ghanem, and O. M. Knio. Multi-resolution analysis of Wiener-type uncertainty propagation schemes. *J. Comput. Phys.*, 197(2):502–531, 2004.

[29] H. G. Matthies and A. Keese. Galerkin methods for linear and nonlinear elliptic stochastic partial differential equations. *Comput. Methods Appl. Mech. Engrg.*, 194(12-16):1295–1331, 2005.

[30] S. Mishra and Ch. Schwab. Sparse tensor multi-level Monte Carlo finite volume methods for hyperbolic conservation laws with random initial data. *Math. Comp.*, 81(280):1979–2018, 2012.

[31] K. Oldham, J. Myland, and J. Spanier. *An atlas of functions*. Springer, New York, second edition, 2009. With Equator, the atlas function calculator, With 1 CD-ROM (Windows).

[32] G. Poëtte, B. Després, and D. Lucor. Uncertainty quantification for systems of conservation laws. *J. Comput. Phys.*, 228(7):2443–2467, 2009.

[33] I. Kröker R. Bürger and C. Rohde. Uncertainty quantification for a clarifier-thickener model with random feed. In *Finite volumes for complex applications VI*, volume 1, pages 195–203. Springer, 2011.

[34] J. F. Richardson and W. N. Zaki. Sedimentation and fluidization: Part i. *Trans. Instn. Chem. Engrs. (London)*, 32:35–53, 1954.

[35] J. R. Shewchuk. Triangle: Engineering a 2D Quality Mesh Generator and Delaunay Triangulator. In Ming C. Lin and Dinesh Manocha, editors, *Applied Computational Geometry: Towards Geometric Engineering*, volume 1148 of *Lecture Notes in Computer Science*, pages 203–222. Springer-Verlag, May 1996. From the First ACM Workshop on Applied Computational Geometry.

[36] J. Tryoen, O. Le Maitre, and A. Ern. Adaptive Anisotropic Spectral Stochastic Methods for Uncertain Scalar Conservation Laws. Technical report, January 2012.

[37] J. Tryoen, O. Le Maître, M. Ndjinga, and A. Ern. Intrusive Galerkin methods with upwinding for uncertain nonlinear hyperbolic systems. *J. Comput. Phys.*, 229(18):6485–6511, 2010.

[38] A. Tveito and R. Winther. The solution of nonstrictly hyperbolic conservation laws may be hard to compute. *SIAM J. Sci. Comput.*, 16(2):320–329, 1995.

[39] D. Xiu and G. E. Karniadakis. Modeling uncertainty in flow simulations via generalized polynomial chaos. *Journal of Computational Physics*, 187(1):137–167, 2003.

Centro de Investigación en Ingeniería Matemática (CI^{2}MA)

PRE-PUBLICACIONES 2012

2012-12 Julio Aracena, Jacques Demongeot, Eric Fanchon, Marco Montalva: *On the number of different dynamics in Boolean networks with deterministic update schedules*

2012-13 Felix Dietzsch, Luis Hervella-Nieto, Steffen Marburg, Rodolfo Rodríguez, Hannah Weisbecker: *Physical and spurious modes in mixed finite element formulation for the Galbrun equation*

2012-14 Emilio Cariaga, Rubén Martínez, Mauricio Sepúlveda: *Estimation of hydraulic parameters under unsaturated flow conditions in heap leaching*

2012-15 Rodolfo Araya, Christopher Harder, Diego Paredes, Frederic Valentin: *Multiscale hybrid-mixed method*

2012-16 Alfredo Bermúdez, Bibiana López-Rodríguez, Rodolfo Rodríguez, Pilar Salgado: *An eddy current problem in terms of a time-primitive of the electric field with non-local source conditions*

2012-17 Gabriel N. Gatica, Antonio Marquez, Walter Rudolph: *A priori and a posteriori error analyses of augmented twofold saddle point formulations for nonlinear elasticity problems*

2012-18 Raimund Bürger, Enrique D. Fernández Nieto, El Hadji Koné, Tomás Morales De Luna: *A multilayer shallow water system for polydisperse sedimentation*

2012-19 Fabián Flores-Bazán, Giandomenico Mastroeni: *Strong duality in cone constrained nonconvex optimization: a general approach with applications to nonconvex variational problems*

2012-20 Alfredo Bermúdez, Dolores Gómez, Rodolfo Rodríguez, Pilar Salgado, Pablo Venegas: *Numerical solution of a transient non-linear axisymmetric eddy current model with non-local boundary conditions*

2012-21 Raimund Bürger, Pep Mulet, Luis M. Villada: *Implicit-explicit methods for diffusively corrected multi-species kinematic flow models*

2012-22 Raimund Bürger, Stefan Diehl: *Convexity-preserving flux identification for scalar conservation laws modelling sedimentation*

2012-23 Raimund Bürger, Ilja Kröker, Christian Rohde: *A hybrid stochastic Galerkin method for uncertainty quantification applied to a conservation law modelling a clarifier-thickener unit*

Para obtener copias de las Pre-Publicaciones, escribir o llamar a: Director, Centro de Investigación en Ingeniería Matemática, Universidad de Concepción, Casilla 160-C, Concepción, Chile, Tel.: 41-2661324, o bien, visitar la página web del centro: `http://www.ci2ma.udec.cl`







Centro de Investigación en
Ingeniería Matemática (CI²MA)
Universidad de Concepción

Casilla 160-C, Concepción, Chile
Tel.: 56-41-2661324/2661554/2661316
http://www.ci2ma.udec.cl